The Plant Cell, Vol. 27: 2860–2879, October 2015, www.plantcell.org

The Transcriptional Repressor MYB2 Regulates Both Spatial and Temporal Patterns of Proanthocyandin and Anthocyanin Pigmentation in *Medicago truncatula*[OPEN]

Ji Hyung Jun,[1] Chenggang Liu,[1] Xirong Xiao, and Richard A. Dixon[2]

Department of Biological Sciences, University of North Texas, Denton, Texas 76203-5017

ORCID IDs: 0000-0002-2563-4144 (J.H.J.); 0000-0002-0576-8567 (C.L.); 0000-0002-1785-6417 (X.X.); 0000-0001-8393-9408 (R.A.D.)

Accumulation of anthocyanins and proanthocyanidins (PAs) is limited to specific cell types and developmental stages, but little is known about how antagonistically acting transcriptional regulators work together to determine temporal and spatial patterning of pigmentation at the cellular level, especially for PAs. Here, we characterize MYB2, a transcriptional repressor regulating both anthocyanin and PA biosynthesis in the model legume *Medicago truncatula*. *MYB2* was strongly upregulated by MYB5, a major regulator of PA biosynthesis in *M. truncatula* and a component of MYB-basic helix loop helix-WD40 (MBW) activator complexes. Overexpression of *MYB2* abolished anthocyanin and PA accumulation in *M. truncatula* hairy roots and *Arabidopsis thaliana* seeds, respectively. Anthocyanin deposition was expanded in *myb2* mutant seedlings and flowers accompanied by increased anthocyanin content. PA mainly accumulated in the epidermal layer derived from the outer integument in the *M. truncatula* seed coat, starting from the hilum area. The area of PA accumulation and *ANTHOCYANIDIN REDUCTASE* expression was expanded into the seed body at the early stage of seed development in the *myb2* mutant. Genetic, biochemical, and cell biological evidence suggests that MYB2 functions as part of a multidimensional regulatory network to define the temporal and spatial pattern of anthocyanin and PA accumulation linked to developmental processes.

INTRODUCTION

Anthocyanins and proanthocyanidins (PAs; also known as condensed tannins) are end products of flavonoid biosynthesis, derived from the phenylpropanoid and acetate/malonate pathways. Both classes of compounds are found as secondary metabolites in a variety of plant species associated with diverse biological and ecological functions (Koes et al., 2005). Anthocyanin pigmentation of various plant organs (flower, leaf, and fruit) aids pollination and seed dispersal and protects against high-light damage (Mouradov and Spangenberg, 2014). Besides their contribution to seed coat pigmentation, PAs are generally considered to act in defense mechanisms against herbivory and fungal pathogens, and the presence of PA has been considered as an important trait in forage crops to prevent pasture bloat and improve nitrogen nutrition in ruminant livestock (Dixon et al., 2005). While both classes of compounds are currently attracting attention due to their medicinal and nutritional values resulting from their antioxidant and organoleptic properties (Dixon et al., 2005), negative effects of high contents of PAs (exceeding 6% of the diet) on animal performance, growth rate, and efficiency of reproduction have been reported (Reed, 1995), and adverse effects on growth and development of transgenic plants with overproduction of PAs using constitutive promoters have also been observed (Sharma and Dixon, 2005). A comprehensive understanding of the biosynthetic and regulatory pathways underlying anthocyanin and PA formation is therefore necessary to ensure that metabolic engineering strategies result in moderate and, therefore, beneficial PA content.

Anthocyanin and PA accumulation is restricted to specific cell types during plant development. Anthocyanins have been shown to accumulate in the epidermal layers of various plant organs (Steyn et al., 2002). In white clover (*Trifolium repens*), staining with dimethylaminocinnamaldehyde (DMACA), a reagent specific for PAs and their flavan 3-ol precursors, was localized to the epidermal cell layer of floral organs in an adaxial-abaxial asymmetric pattern (Abeynayake et al., 2011). PA accumulation is also often found specifically in trichomes on plant organs with relatively low PA levels (Hancock et al., 2012). In *Arabidopsis thaliana*, PAs are exclusively synthesized and accumulated in the seed coat and localized in endothelial cells derived from the inner integument (Debeaujon et al., 2003). As flavonoid intermediates and precursors are highly reactive and potentially toxic to plant cells, it seems important that plants restrict the accumulation of these compounds to specialized cell types to avoid damage during development and to respond effectively to environmental cues.

Both the anthocyanin and PA biosynthetic pathways have been well defined through studies of mutants lacking the pigments in many model species (Lepiniec et al., 2006) and the genes required for biosynthesis are regulated in a tissue-specific manner as well as by a variety of environmental signals (Albert et al., 2009). Early steps of the biosynthetic pathways are shared by anthocyanins and PAs before anthocyanidin is modified by glycosylation, acylation, and/or methylation to produce diverse anthocyanins or reduced to generate the flavan 3-ol PA precursor (epicatechin) by ANTHOCYANIDIN REDUCTASE (ANR) and glycosylation by glucosyltransferase (Xie et al., 2003; Pang et al., 2008). An

[1] These authors contributed equally to this work.
[2] Address correspondence to richard.dixon@unt.edu.
The author responsible for distribution of materials integral to the findings presented in this article in accordance with the policy described in the Instructions for Authors (www.plantcell.org) is: Richard A. Dixon (richard.dixon@unt.edu).
[OPEN] Articles can be viewed online without a subscription.
www.plantcell.org/cgi/doi/10.1105/tpc.15.00476

alternative PA monomer (catechin) is believed to be produced from leucoanthocyanidin by LEUCOANTHOCYANIDIN REDUCTASE (LAR) (Tanner et al., 2003). The proteins involved in trafficking of anthocyanin or PA monomers into the vacuole, and their polymerization, have been reported (Goodman et al., 2004; Zhao and Dixon, 2009) (Supplemental Figure 1). Biosynthesis of many of these proteins has been found to be regulated by MBW complexes composed of R2R3-MYB, R/B-like basic helix-loop-helix (bHLH), and WD40 repeat factors (Supplemental Figure 1; Ramsay and Glover, 2005). MBW complexes are also known to regulate development of trichomes and root hairs and accumulation of seed mucilage in Arabidopsis, and specific combinations of MYB and bHLH with WD40 regulate the specific pathways for PA or anthocyanin biosynthesis through physical interaction between these three components (Lepiniec et al., 2006). The structural genes for anthocyanin or PA pathway enzymes are coordinately activated. Among the R2R3 factors, PAP1, PAP2, MYB113, and MYB114 are known to redundantly regulate anthocyanin production by regulating anthocyanin biosynthetic genes *F3′H*, *DFR*, *ANS*, and *UFGT* (Gonzalez et al., 2008). Accumulating data show direct regulation of PA biosynthetic genes, including *CHS*, *F3H*, *F3′H*, *DFR*, *LDOX*, *ANR*, *GST* (*TT19*), and *MATE* (*TT12*), and the H^+ ATPase gene *AHA10* by TT2/MYB5-TT8/GL3/EGL3-TTG1 MBW complexes in Arabidopsis (Xu et al., 2014).

In *Medicago truncatula*, PA accumulation is almost exclusively detected in the seed coat from the earliest measurable stage of seed development (Pang et al., 2007), and purple anthocyanin pigmentation is observed in various organs from the seedling to reproductive stage (Pang et al., 2009). Mt WD40-1 (a functional ortholog of At TTG1) was identified from a mutant screen; the *wd40-1* mutant lacked the typical red pigmentation in vegetative tissues and browning of the seed coat, indicating that WD40-1 is involved in both the PA and anthocyanin pathways (Pang et al., 2009). Three R2R3 MYB proteins (Mt PAR, Mt MYB14, and Mt MYB5) have been reported to regulate the PA pathway in seeds of *M. truncatula* (Verdier et al., 2012; Liu et al., 2014), and so far the only R2R3 MYB known to be involved in anthocyanin biosynthesis is Mt LAP1 (Peel et al., 2009) (Supplemental Figure 1). Recent data also showed that synergistic physical interactions between MYB14 and MYB5 enhance transcription of target PA pathway genes such as *ANR* (Liu et al., 2014), indicating that *M. truncatula* has a quaternary complex system to regulate PA accumulation in the seed coat, the extra component, MYB5, not being a major regulator of PA biosynthesis in Arabidopsis (Li et al., 2009).

Because anthocyanin and PA accumulation are only detected in specific tissues and developmental stages or under certain environmental conditions, and expression of some of the required genes is regulated by both developmental and environmental regulatory machineries, regulation of pathway-specific transcription factors appears to be critical for production of specific compounds in different cellular contexts. In addition to the spatial and temporal regulation of transcription, as shown with seed coat-specific expression of *TT2* (Gonzalez et al., 2009), key amino acids in MYB transcription factors for target promoter specificity were found between TT2-type and PAP4-type MYB proteins (Heppel et al., 2013). The switching mechanism of a dimerization domain in a bHLH factor to permit distinct configurations of a regulatory complex for binding on different promoters was also reported (Kong et al., 2012). To add to the complexity of MBW activity regulation, several anthocyanin repressors including small R3 MYBs (CPC, ETC1, and MYBx), MYBL2 with partial R2 and complete R3 domain, and subgroup 4 R2R3 MYBs (Fa MYB1 and Fc MYB1 from strawberry [*Fragaria* spp] and Ph MYB27 from petunia [*Petunia hybrida*]), have been characterized (Aharoni et al., 2001; Dubos et al., 2008; Zhu et al., 2009; Salvatierra et al., 2013; Albert et al., 2014; Nemie-Feyissa et al., 2014). R3 MYBs, which contain only an R3 domain and no repressive motif, are known to function as passive repressors by competing with R2R3 MYB activators for binding to a bHLH partner (Guimil and Dunand, 2006). MYBL2 from Arabidopsis and subgroup 4 R2R3 MYBs contain a repression motif (TLLLFR) or an ERF-associated amphiphilic repression (EAR) motif in their C termini to actively repress transcription (Matsui et al., 2008; Albert et al., 2014). Direct interaction of MYBL2 and Ph MYB27 with bHLH proteins (TT8 and AN1/JAF13) was shown, and ternary complex formation of Ph MYB27-AN1/JAF13-DPL indicates that Ph MYB27 may act as a corepressor by being incorporated into MBW activator complexes (Matsui et al., 2008; Albert et al., 2014). In Arabidopsis, *MYBL2* promoter activity is expressed in the endothelium of the seed coat, and expression of *MYBL2* driven by the *TT8* promoter produced seeds with reduced PA content (Dubos et al., 2008). Overexpression of Fa *MYB1*, grapevine (*Vitis vinifera*) Vv *MYBC2*, or poplar (*Populus trichocarpa*) Ptr *MYB182* resulted in reductions of PA or both PA and anthocyanin biosynthesis (Paolocci et al., 2011; Huang et al., 2014; Yoshida et al., 2015; Cavallini et al., 2015). However, information on how MYB repressors may be involved in fine spatio-temporal regulation of pigmentation is still limited, especially for PA deposition, and requires analysis of loss-of-function phenotypes.

Here, we show that Mt MYB2 acts as a transcriptional repressor in the regulation of both anthocyanin and PA levels and distribution by targeting both EBGs (early biosynthetic genes involved in the biosynthesis of the common precursors of three classes of flavonoids) and LBGs (late biosynthetic genes) in *M. truncatula*. We define the pattern of PA accumulation in the *M. truncatula* seed coat at the cellular level and find that combined activity of MYB2 and MBW (MYB14/MYB5-TT8-WD40-1) complexes contributes to tight regulation of the progression of PA deposition during *M. truncatula* seed coat development. Our data also suggest that different inhibitory activities of MYB2 against diverse combinations of R2R3 MYB activators in MBW complexes is one of the fine-tuning mechanisms for the PA pathway. A model of MYB2 function in pattern formation of secondary metabolite biosynthesis linked to seed developmental processes is proposed.

RESULTS

Identification of Mt MYB2 in *M. truncatula*

Recently, Mt MYB5 was identified as major regulator of the PA biosynthetic pathway in *M. truncatula*, and Medtr5g079670, a putative repressor, was found as one of the most highly induced genes in hairy roots generated from *M. truncatula* A17 plants overexpressing *MYB5* (Figure 1A; Liu et al., 2014). Since Medtr5g079670 encodes a 213-amino acid R2R3 MYB transcription

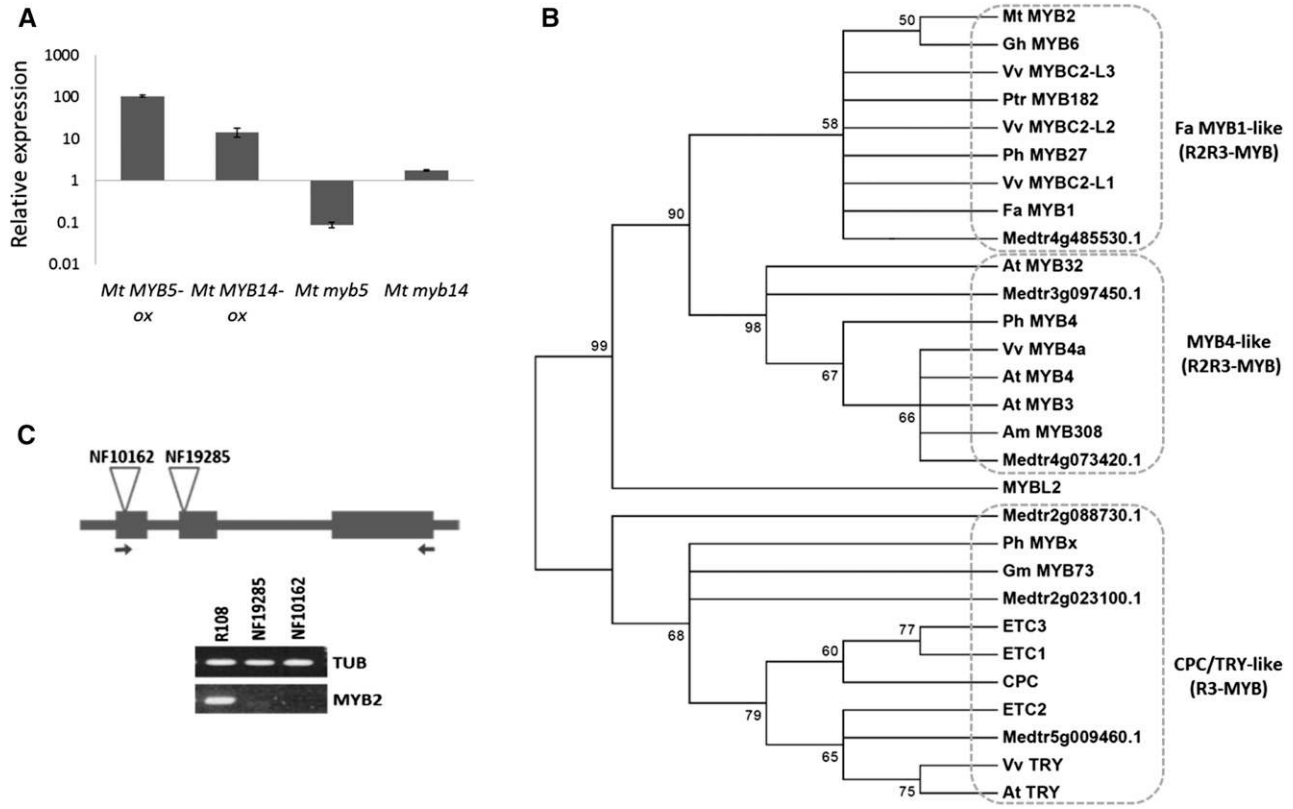

Figure 1. Identification of *M. truncatula* MYB2.

(A) Microarray analysis of Mt *MYB2* (probe set ID Mtr.34401.1.S1_s_at) expression in *M. truncatula* hairy roots overexpressing Mt *MYB14* and Mt *MYB5* and in Mt *myb5* and Mt *myb14* mutant seeds. Microarray experiments were performed on three and two independent biological replicates for hairy roots and mutants, respectively. The relative expression was calculated with normalization to tubulin (probe set ID Mtr.40026.1.S1_at). Error bars indicate standard deviations.

(B) Phylogenetic tree of repressor MYB transcription factors based on the N-terminal protein sequences including R2R3 domain or only R3 domain for small MYB proteins. The phylogenetic tree was constructed using MEGA 6 (Tamura et al., 2013) with 1000 bootstrap replicates. Numbers indicate the percentage of consensus support.

(C) *Tnt1* retrotransposon insertion positions in the Mt *MYB2* gene. Arrows indicate the insertion positions in *myb2-1* (NF10162) and *myb2-2* (NF19285). Solid boxes indicate exons and thinner lines indicate introns. The positions of primer pairs used for the PCR (bottom panel) are shown by arrows.

factor that shows highest sequence identity with the anthocyanin repressor MYBL2 among *M. truncatula* MYB proteins, and MYBL2 was also found to be a downstream target of Arabidopsis MYB5 (Dubos et al., 2008; Li et al., 2009), we named Medtr5g079670 as Mt MYB2. *MYB2* transcript level was strongly reduced in *myb5* mutant seeds (Figure 1A). *MYB2* expression was also highly induced by overexpression of the PA regulator *MYB14* in *M. truncatula* hairy roots and overexpression of the anthocyanin regulator Mt *LAP1* in transgenic plants of alfalfa (*Medicago sativa*) (Figure 1A; Supplemental Figure 2). The transcript level of *MYB2* was not reduced in *myb14* mutant seeds (Figure 1A).

In a phylogenetic analyses of repressor MYB proteins based on N-terminal protein sequences encompassing the R2R3 domain or R3 domain (for the R3-MYB group) or the entire protein sequences (Figure 1B; Supplemental Figures 3 and 4 and Supplemental Files 1 and 2), MYB2 was clustered with a group of proteins that have been identified as negative regulators of anthocyanin and/or PA biosynthesis in other plant species (Aharoni et al., 2001; Albert et al., 2014; Yoshida et al., 2015; Cavallini et al., 2015). One R2R3 MYB protein, MYB 530 (Medtr4g485530.1) from *M. truncatula* was also found in the same clade, which is separated from the MYB4 lignin/phenylpropanoid MYBs. Protein sequence alignment of the Fa MYB1-like proteins and MYBL2 indicates that the R2 domain and R3 domain containing the bHLH interaction residue ([DE]Lx2[RK]x3Lx6Lx3R; Zimmermann et al., 2004) are highly conserved and all of the proteins except Fa MYB1 additionally contain the C1 motif (LlsrGIDPxT/SHRxl/L; Shen et al., 2012) (Supplemental Figure 5). More importantly, a putative EAR-like repressive motif (LxLxL) is present near the C-terminal end of the proteins. Some of the Fa MYB1-like proteins, such as cotton (*Gossypium hirsutum*) Gh MYB6 and Vv MYBC2, additionally contain a TLLLFR repression domain that was originally identified in MYBL2. MYB2 does not have a TLLLFR domain but instead possesses a semi-conserved EAR sequence at the C-terminal end in addition to a canonical EAR motif in the C2 domain (pdLNLD/ELxiG/S; Shen et al., 2012) (Supplemental Figure 5).

In the microarray data of the *Medicago truncatula* Gene Expression Atlas (http://mtgea.noble.org/v2/probeset.php?id=Mtr.34401.1.S1_s_at) obtained using the probe set Mtr.34401.1.S1_s_at as query, *MYB2* transcripts are strongly expressed in flower and developing seeds, and this expression pattern is highly overlapping with the expression profile of *MYB5* (Liu et al., 2014), suggesting that MYB2 might have roles as a negative regulator of MBW complexes in these tissues.

Mt MYB2 Is a Negative Regulator of Anthocyanin Biosynthesis

To better understand the functions of MYB2, we screened the *Tnt1* retrotransposon mutagenized *M. truncatula* R108 population (Tadege et al., 2008). Two independent MYB2 *Tnt1* insertion lines were isolated. *Tnt1* insertions were located in the first and second exon of the *MYB2* gene in lines NF10162 and NF19285, respectively (Figure 1C). RT-PCR could not detect the full-length *MYB2* transcript in either line, indicating that they are null mutants (Figure 1C). No morphological phenotypic differences between mutant and wild-type plants were detected during the entire developmental period under our growth conditions, and both lines were used for further analysis.

At the seedling stage, *myb2* mutants showed more anthocyanin accumulation in hypocotyl, junction of hypocotyl and root, and occasionally abaxial side of true leaves compared with the wild type when plants were grown on Murashige and Skoog medium (Figure 2A, top panel). Expanded anthocyanin accumulation was also observed in the flower of *myb2* mutant plants. The flower banner of wild-type *M. truncatula* R108 had only a small spot of anthocyanin accumulation in the center, whereas the mutants exhibited a circular purple area around the fused keel petal (Figure 2A, bottom panel). The *myb2* plants accumulated ~2.5- and 1.7-fold more anthocyanin than the wild type in seedling and flower, respectively (Figure 2B). However, purple spots on the adaxial surface of leaf and stem epidermal cells did not show any change in number, spot size, or color intensity of anthocyanin pigmentation, indicating that MYB2 function might be required under specific environmental conditions in these tissues or have functional redundancy with other anthocyanin suppressors during vegetative growth.

To demonstrate that MYB2 can inhibit anthocyanin accumulation in planta, we generated *MYB2*-overexpressing transgenic hairy roots in *M. truncatula* ecotype A17. The purple anthocyanin accumulation characteristic of wild-type roots was absent in the *MYB2*-overexpressing roots (Figure 2C). Some lines of *MYB2*-transformed hairy roots showed retarded growth (Figure 2C, MYB2-ox-2). The anthocyanin level was highly reduced in both overexpression lines, and this correlated with suppression of *ANS* and *DFR1* transcript levels (Figures 2D and 2E). To gain insights into MYB2-regulated genes in *M. truncatula*, three independent biological replicates of *MYB2*-expressing and vector control hairy roots were subjected to transcriptome analysis using Affymetrix *M. truncatula* GeneChips. In total, 326 and 226 probe sets were identified to be induced and suppressed in *MYB2*-overexpressing hairy roots, respectively (transcript ratio of >2 or <0.5; $P < 0.05$) (Supplemental Data Set 1). According to GeneBins ontology (Goffard and Weiller, 2007), 20 probe sets of genes that were repressed in the MYB2 hairy roots encode enzymes involved in the biosynthesis of secondary metabolites (Table 1; Supplemental Figure 6). An acyltransferase (probe set ID Mtr.44986.1.S1_at) that is annotated as malonyl-CoA:isoflavone 7-*O*-glucoside malonyltransferase (Medicago genome 4.0 Medtr6g015830.1) and possibly involved in modification of anthocyanin was identified as the most repressed transcript (Table 1; 25-fold reduction), and transcripts encoding characterized enzymes required for flavonoid biosynthesis, including DFR1 and 2, F3′H, ANS (Medtr5g011250.1), CHS, and UGT78G1, were also affected, indicating that MYB2 plays a role as a general suppressor of anthocyanin biosynthesis (Table 1). The changes in expression of a selection of these genes was confirmed with qRT-PCR, and, in addition, strong reduction of *TT8* transcript levels and mild reduction of *MYB5* transcripts were found (Supplemental Figure 7). These latter genes were not represented in the microarray data.

Target gene expression was also analyzed in wild-type and mutant seedlings at 7 d after germination. *CHS1*, *DFR1*, *ANS*, and *F3H* were upregulated in *myb2* seedlings (Figure 2F). *DFR2* expression was not detected in either wild-type or *myb2* mutant seedlings. *TT8* and *MYB5* expression were also increased in the *myb2* mutant, as was expression of *MYB530*, which was identified as the closest homolog of MYB2 in the *Medicago* genome. This indicates that regulators of the anthocyanin pathway genes are also regulated by MYB2 (Figure 2F).

MYB2 Is a Negative Regulator of PA Biosynthesis

To determine if mutations in MYB2 have an effect on PA accumulation, we observed the seed color during the entire program of seed growth and maturation. There was no difference detected between the wild type and mutant alleles in the color of the seed coat from bright green to brown during seed development to desiccation (Figure 3A). However, staining with DMACA indicated more accumulation of PAs and/or their flavan-3-ol precursors in the *myb2* mutant seed coat (Figure 3B). Wild-type seeds at 10 DAP (days after pollination) only accumulated purple/blue-staining PA around the hilum area. The staining was restricted to the same area at 12 DAP but then began to expand to the seed body until staining covered the entire seed coat at 20 DAP. At this time, the hilar groove had stronger staining than other areas, but staining then became evenly distributed and saturated by 30 DAP. Expansion of DMACA staining started earlier and was always stronger on the micropyle side compared with the chalazal side before 20 DAP in wild-type seeds (Figure 3B). In *myb2* mutant seeds, DMACA staining was already detected in half of the seed body from the hilar side at 12 DAP (Figure 3B), and it covered the whole seed coat from 14 DAP although the staining was stronger in the hilar area (proximal side) as also seen in the wild-type seed coat (Figure 3B). The staining was stronger in both mutant alleles through seed development compared with the wild type, but we could not see a difference in mature seed (from 30 DAP) due to the saturation of DMACA staining (Figure 3B). Since it has been shown that the *wd40-1* mutant from *M. truncatula* has a defect in PA biosynthesis (Pang et al., 2009), the seed staining phenotype of the *wd40-1* mutant was analyzed in parallel. The dry seeds from *wd40-1* plants showed a yellowish seed color (Figure 3A) and no purple/blue staining was detected with DMACA (Figure 3B); this confirms that the purple/blue staining in the wild type and *myb2* mutant is indeed due to PAs.

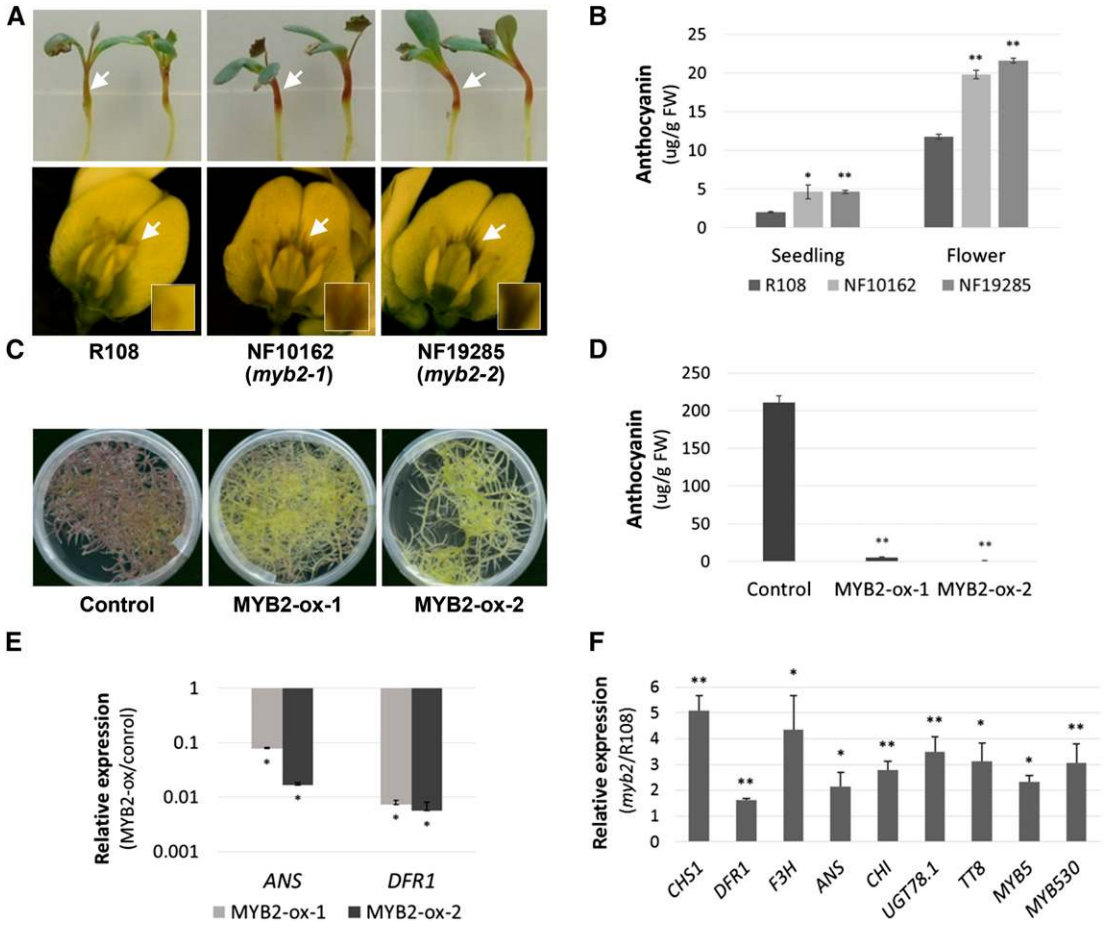

Figure 2. MYB2 Is a Negative Regulator of Anthocyanin Biosynthesis.

(A) Phenotypes of *myb2-1* (NF10162) and *myb2-2* (NF19285). Arrows indicate anthocyanin accumulation in the hypocotyl (7-d-old seedlings, top panel) and in the middle of banner petals (bottom panel). Magnified views of areas of anthocyanin accumulation are shown in the boxes.

(B) Anthocyanin levels in *myb2* mutants. Error bars represent SD of three biological replicates. **P < 0.01 and *P < 0.05, Student's *t* test.

(C) Phenotypes of *M. truncatula* (A17) hairy root cultures of vector control and two independent transgenic *MYB2* overexpression lines. Purple color of control line indicates accumulation of anthocyanin.

(D) Anthocyanin levels in *M. truncatula* (A17) hairy root cultures. Data are means ± SD ($n = 3$). **P < 0.01, Student's *t* test.

(E) qRT-PCR analysis of transcript levels in transgenic *MYB2* overexpression lines in **(C)** compared with control. Data are means ± SD of three biological replicates with two technical replicates. *P < 0.01, Student's *t* test.

(F) qRT-PCR analysis of transcript levels in *myb2* seedlings (7 d old) compared with control R108. Data are means ± SD of three biological replicates with two technical replicates. **P < 0.01 and *P < 0.05, Student's *t* test.

To quantify PA accumulation, we extracted soluble and insoluble (nonextractable) PAs separately. Soluble PA levels were significantly increased in *myb2* mutant seeds at every stage of development, including 30 DAP and dry (40 DAP) seeds, with a fold-change increase of ~1.5 in mutants compared with the wild type (Figure 3C). Soluble PA level was also increased in flowers and young pods at 4 to ~6 DAP, although the absolute level of PA was low (<20 μg epicatechin equivalents g^{-1} fresh weight) (Supplemental Figure 8). Measurement of insoluble PA based on butanol-HCl hydrolysis showed that *myb2* mutants have more nonextractable PAs at 16, 20, and 30 DAP (Figure 3D). No significant difference was detected in seeds at 12 and 40 DAP.

To determine whether the composition of soluble PA was altered in mutant seeds, size heterogeneity of soluble PAs was determined by normal-phase HPLC coupled to postcolumn derivatization with DMACA reagent (Peel and Dixon, 2007). At 16 DAP, both wild-type and *myb2* mutant seeds had low levels of free epicatechin monomer along with a range of oligomers (Supplemental Figure 9). In 30 DAP and dry seeds, free monomers were not detected and most of the soluble PA fraction was shifted to a higher degree of polymerization, leaving only a trace amount of smaller units in dry seeds (Figure 3E; Supplemental Figure 9). At all three developmental stages, the *myb2* mutant produced a similar profile but higher amounts of PA compared with the wild type, indicating no major change in the size of soluble PAs in the *myb2* mutant (Figure 3E; Supplemental Figure 9).

Table 1. Flavonoid Pathway Gene Probe Sets That Were Downregulated More Than 2-Fold by *MYB2* Overexpression in *M. truncatula* (A17) Hairy Roots

Probe Set	Target Description	Ratio (MYB2/CK)	P Value[a]	Q-Value[b]
Mtr.44986.1.S1_at	Similar to UP|Q9FID1 (Q9FID1) Acyltransferase-like protein (At5g39090), partial (13%)	0.04	0	0.008314000
Mtr.38073.1.S1_at	UP|Q6TQT1 (Q6TQT1) Dihydroflavanol-4-reductase 1, complete	0.06	0	0.001435000
Mtr.6517.1.S1_at	Similar to UP|Q84J65 (Q84J65) Gray pubescence flavonoid 3′-hydroxylase, partial (49%)	0.09	0	0.015502818
Mtr.37182.1.S1_s_at	Similar to GB|BAB02518.1|11994477|AB028618 anthocyanin 5-aromatic acyltransferase/ benzoyltransferase-like protein (*Arabidopsis thaliana*), partial (17%)	0.09	0	0.007902000
Mtr.36333.1.S1_at	Similar to UP|Q84JJ4 (Q84JJ4) Flavonoid 3′-hydroxylase (fragment), partial (21%)	0.10	0	0.000445000
Mtr.38756.1.S1_at	UP|Q6TQT0 (Q6TQT0) Dihydroflavonal-4-reductase 2, complete	0.12	8.23433E-20	0.006686000
Mtr.28774.1.S1_at	Similar to UP|Q6PTC5 (Q6PTC5) Anthocyanidin synthase, partial (53%)	0.13	0	0.000711000
Mtr.3858.1.S1_at	Similar to UP|Q6BEG9 (Q6BEG9) Leucoanthocyanidin dioxygenase, partial (24%)	0.21	0	0.000172000
Mtr.49421.1.S1_at	2OG-Fe(II) oxygenase AC138453.8.	0.29	0	0.001659000
Mtr.39747.1.S1_at	Weakly similar to UP|Q9AR45 (Q9AR45) UDP-glucose: flavonoid 3-*O*-glucosyltransferase, partial (35%)	0.29	3.51499E-55	0.018529000
Mtr.13746.1.S1_at	Weakly similar to UP|Q9FI39 (Q9FI39) Cytochrome P450, partial (25%)	0.32	0	0.000637535
Mtr.28714.1.S1_at	Homolog to PRF|1609233A|226868|1609233A chalcone synthase 3 (*Sinapis alba*), partial (12%)	0.36	3.35642E-35	0.003032000
Mtr.14428.1.S1_at	Naringenin-chalcone synthase; Type III polyketide synthase AC146683.9	0.39	0	0.006988000
Mtr.50800.1.S1_at	2OG-Fe(II) oxygenase	0.43	1.48152E-41	0.011693957
Mtr.45963.1.S1_at	*O*-methyltransferase, family 2; Generic methyltransferase; SAM (and some other nucleotide) binding motif	0.43	5.1614E-98	0.004453447
Mtr.17487.1.S1_s_at	E-class P450, group I; Cytochrome P450	0.46	0	0.000281424
Mtr.19945.1.S1_at	Anthocyanin acyltransferase	0.46	0	0.000361000
Mtr.44766.1.S1_at	Similar to UP|Q9ZQW2 (Q9ZQW2) Laccase, partial (42%)	0.47	1.08057E-38	0.018890000
Mtr.20567.1.S1_at	Type III polyketide synthase; Naringenin-chalcone synthase	0.49	1.797E-216	0.068801000
Mtr.31382.1.S1_at	Dihydroflavonol 4-reductase	0.51	6.61032E-41	0.169790000

Expression values were obtained by robust multichip averaging (Irizarry et al., 2003).
[a]Obtained using associate analysis (Dozmorov and Centola, 2003).
[b]Obtained using EDGE (Leek et al., 2006).

Phloroglucinolysis analysis (Pang et al., 2007) was then used to determine the monomeric composition and mean degree of polymerization after purification of the soluble PAs on Sephadex LH20 resin. Although quantitatively more PA was observed from *myb2* mutants by this method, the polymers in both the wild type and mutant released similar proportions of phloroglucinol-epicatechin extension units and epicatechin starter units, with similar mean degrees of polymerization (wild type, 15.95 ± 0.49; *myb2*, 17.05 ± 1.77 in dry seeds) (Figure 3F; Supplemental Figure 10). These data indicate that MYB2 influences the quantity but not the quality of PAs in *M. truncatula* seeds.

We next analyzed transcript levels of PA pathway genes in 12 DAP seeds dissected from pods of wild-type and mutant plants. qRT-PCR results showed that many of the PA biosynthetic pathway genes were upregulated in *myb2* mutant seeds. EBGs including *CHS1*, *F3H*, and *F3′H* showed more than 2-fold increases and a smaller but significant induction of *ANS* was also detected. The transcript level of *LDOX* (Medtr3g072810.1), which is a homolog of *ANS* (Medtr5g011250.1) and was previously identified as a downstream target of MYB14 and MYB5 (Liu et al., 2014), was highly increased in the *myb2* mutant. Among the LBGs, the homolog of Arabidopsis *TT19* was induced more than 2-fold, and *ANR*, *LAR*, *UGT72L1*, and *MATE1* expression were also upregulated. Interestingly, the most highly differentially expressed gene was *MYB730* (Medtr2g088730.1), which was identified as encoding a small R3-MYB in an *M. truncatula* genome search and the close homolog of *CPC*. We also observed increases in *MYB530* and *TT8* transcript levels in *myb2* seeds (Figure 3G).

To test if MYB2 can inhibit PA accumulation, transgenic Arabidopsis plants were generated using an *MYB2* overexpression construct. Transgenic plants produced seeds with yellow seed coat color (Figure 3H; Supplemental Figure 11A), and qRT-PCR results

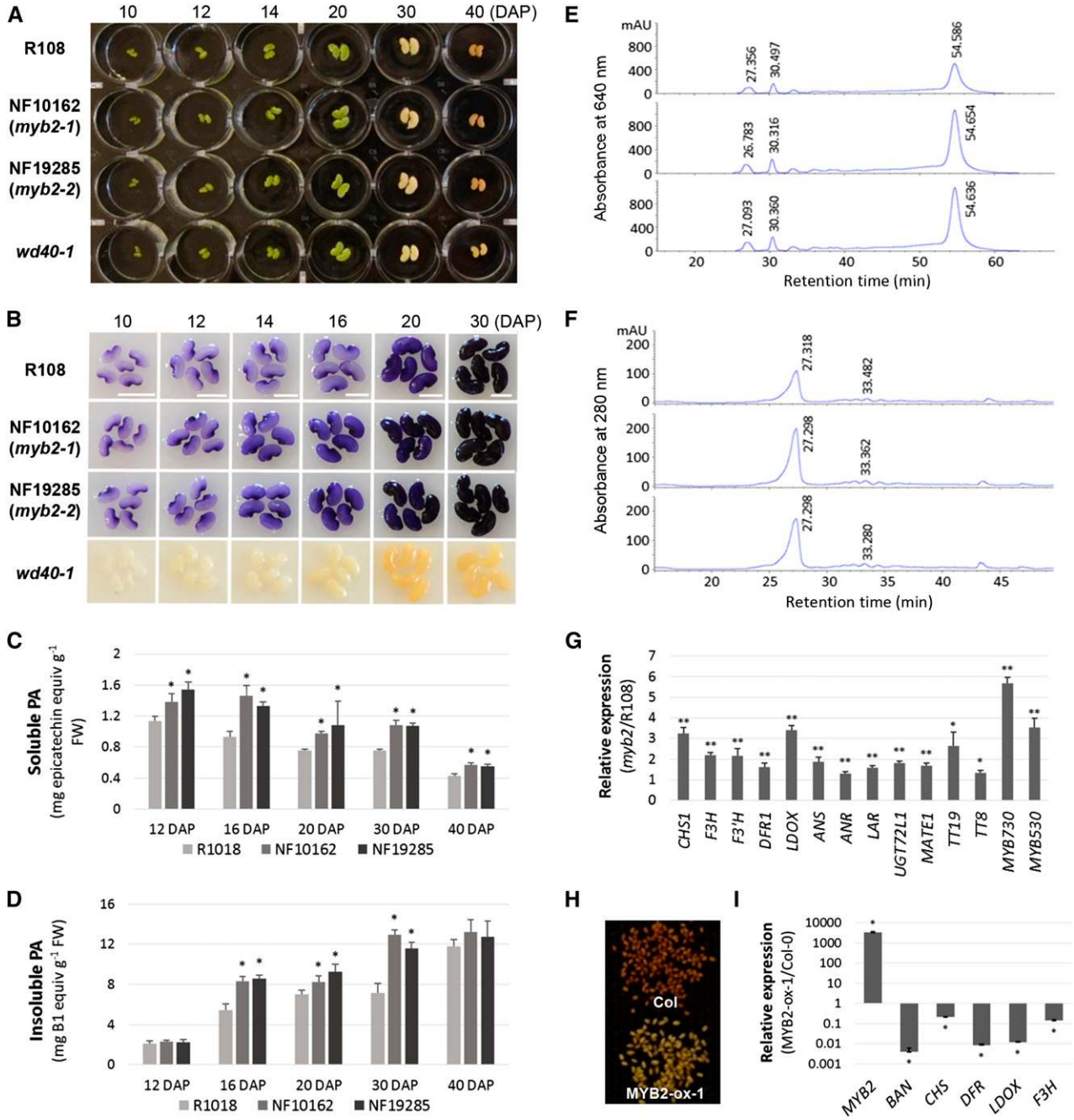

Figure 3. MYB2 Is a Negative Regulator of PA Biosynthesis.

(A) Phenotypes of wild type (R108), *myb2-1* (NF10162), *myb2-2* (NF19285), and *wd40-1* (NF0977) mutants during seed development.

(B) DMACA-stained seeds of wild type (R108), *myb2-1* (NF10162), *myb2-2* (NF19285), and *wd40-1* (NF0977) mutants. Bars = 2 mm.

(C) Soluble PA levels as quantified with DMACA reagent and expressed as epicatechin equivalents. Data are means ± SD ($n = 6$, three biological replicates). *$P < 0.01$, Student's *t* test.

(D) Insoluble PA levels as quantified by the butanol-HCl method and expressed as procyanidin B1 equivalents. Data are means ± SD ($n = 6$, three biological replicates). *$P < 0.01$, Student's *t* test.

(E) Normal-phase HPLC analysis, with postcolumn derivatization with DMACA, of soluble PA fractions from wild-type (top), *myb2-1* (middle), and *myb2-2* (bottom) seeds at 30 DAP. Retention time for the major peaks is noted.

(F) Phloroglucinolysis analysis of 30 DAP seeds of wild-type (top), *myb2-1* (middle), and *myb2-2* (bottom) plants. Retention time for phloroglucinol-epicatechin and epicatechin is noted.

showed that expression of PA pathway genes, including *BAN* (*ANR*), were highly reduced in young siliques (Figure 3I; Supplemental Figure 11B). *MYB2* overexpression lines failed to accumulate anthocyanin in the base of the cotyledon and hypocotyl at the seedling stage. *MYB2*-overexpressing plants also had no anthocyanin at the bases of the primary stem and side branches, but showed normal trichome development on stems (Supplemental Figures 11C and 11D). Thus, ectopic expression of *MYB2* suppresses both PA and anthocyanin biosynthesis in Arabidopsis.

Molecular Mechanism of MYB2 in Relation to MBW Complexes

We have previously shown that a MYB5-TT8-WD40-1 complex can activate the *M. truncatula ANR* promoter directly in Arabidopsis protoplasts in dual luciferase assays (Liu et al., 2014). To test whether MYB2 can suppress MBW complex activity by virtue of the EAR motif found in its C-terminal region (LNLDL, residues 180 to 184), MYB2 or MYB2_m1, in which the three Leu residues were changed to Ala (ANADA), was cotransfected into Arabidopsis protoplasts along with various combinations of MBW components. Whereas intact MYB2 could suppress *ANR* promoter activity down to as low as 4% of control activity when coexpressed with MYB5-TT8-WD40-1 constructs, *ANR* promoter activation was only partially suppressed when the mutated version of MYB2 was included (50% induction of the activity without MYB2) (Figures 4A and 4B). Since a semiconserved EAR motif sequence (MDIDL, residues 207 to 211) was also found at the C-terminal end of the MYB2 protein, we introduced a second mutation (MYB2_m2) by exchanging the Ile and Leu residues with Ala (MDADA) (Figure 4A). This replacement alone relieved MYB2 repression to a lesser extent compared with the mutation in MYB2_m1, but combination of the mutations in both potential suppressive domains completely abolished MYB2 repressive activity on the *ANR* promoter (Figure 4B). The same result was observed with different promoters (LAR_{pro}, $CHS1_{pro}$, $LDOX_{pro}$, and $DFR1_{pro}$) that are known to be direct targets of TT2/MYB5-TT8-TTG1 complexes in Arabidopsis (Figure 4C). MYB2_m1m2-AD (Gal4 DNA activation domain) fusion protein did not itself activate the *ANR* promoter, indicating that MYB2 protein itself may not bind directly to the promoter (Figure 4B).

To test physical interactions between MYB2 and MBW components, bimolecular fluorescence complementation (BiFC) assays were performed in Arabidopsis protoplasts. The complementary eYFP signal was only observed when MYB2 and TT8 constructs were cotransfected, whereas MYB2 did not show any interaction with MYB5, MYB14, or WD40-1 proteins (Figure 4D; Supplemental Figure 12). However, MYB2 also showed a TT8-dependent interaction with MYB5 or MYB14 (Figure 4D; Supplemental Figure 12), indicating that MYB2 can be incorporated in the MBW complex by making physical interactions with MYB5 or MYB14 that result in an inhibitory complex and that are mediated by TT8. This conclusion is further supported by the efficient suppression of promoter activity by MYB2 when TT8 was cotransfected (Figure 4B; Supplemental Figure 13). No dilution effect of MYB2_m1m2 on MYB5 activity in transactivation assays indicates that MYB2 functions as an active inhibitor rather than as a passive competitor, since MYB2_m1m2 protein interacts normally with TT8 (Figures 4B and 4D). However, the fact that MYB2_m1m2-AD fusion protein did not enhance *ANR* promoter activity when combined with MYB5 (Figure 4B), in contrast to the case of synergistic promoter activation upon cotransfection of MYB5 and MYB14 (Liu et al., 2014), suggests that a specific configuration of the activator complex is required upon binding to the target promoter to enhance transcription.

To define the inhibitory mechanism of MYB2 on MYB5 or MYB14 MBW complexes, dosage-dependent suppression of *ANR* promoter activity was tested. When serial dilutions of MYB2 construct were cotransfected along with different MBW complexes, the MBW MYB14-TT8-WD40-1 complex showed the most sensitive response to low concentrations of MYB2 (more than 50% reduction at the ratio of MYB14 to MYB2 of 1:0.03125) compared with MYB5-TT8-WD40-1 and MYB5-MYB14-TT8-WD40-1 combinations, which had similar 20% reductions (Figure 4E). Since the fold induction of promoter activity with MYB5-MYB14-TT8-WD40-1 combinations compared with no effector was the highest (747.7-fold; Supplemental Figure 14), these data indicate that coregulation of target promoters by MYB5 and MYB14 has an additive effect in terms of transcriptional activation and resistance to repressor(s), which is mainly attributed to the presence of MYB5 (Figure 4F).

Spatio-Temporal Regulation of PA Accumulation by MYB2 in *M. truncatula* Seeds

To determine the spatio-temporal patterns of PA accumulation in *myb2* mutant seeds, detailed histochemical analysis was performed at different stages of seed development. Longitudinal sections from wild-type and *myb2-1* (NF10162) seeds were stained with toluidine blue O (TBO), which was reported to show specific greenish-blue staining indicating deposition of PA or PA precursors in Arabidopsis (Debeaujon et al., 2003). The green staining was localized to the seed coat, but it was mainly detected in the epidermal cell layer on the hilar side of the seed coat (Supplemental Figure 15), while it was observed in the endothelium of the Arabidopsis seed coat (Debeaujon et al., 2003). In the hilar groove and the proximal region close to the micropyle and embryo, the vacuoles at the bottom of the epidermal cells were

Figure 3. (continued).

(G) qRT-PCR analysis of transcript levels in *myb2* seeds (12 DAP) compared with control R108. Data are means ± SD of three biological replicates with two technical replicates. **P < 0.01 and *P < 0.05, Student's *t* test.

(H) Seed coat phenotypes of control (Col-0) and *MYB2* overexpressing Arabidopsis plants.

(I) qRT-PCR analysis of transcript levels in *MYB2*-overexpressing Arabidopsis plants compared with control. Young siliques were used for analysis. Data are means ± SD of three biological replicates with two technical replicates. *P < 0.01, Student's *t* test.

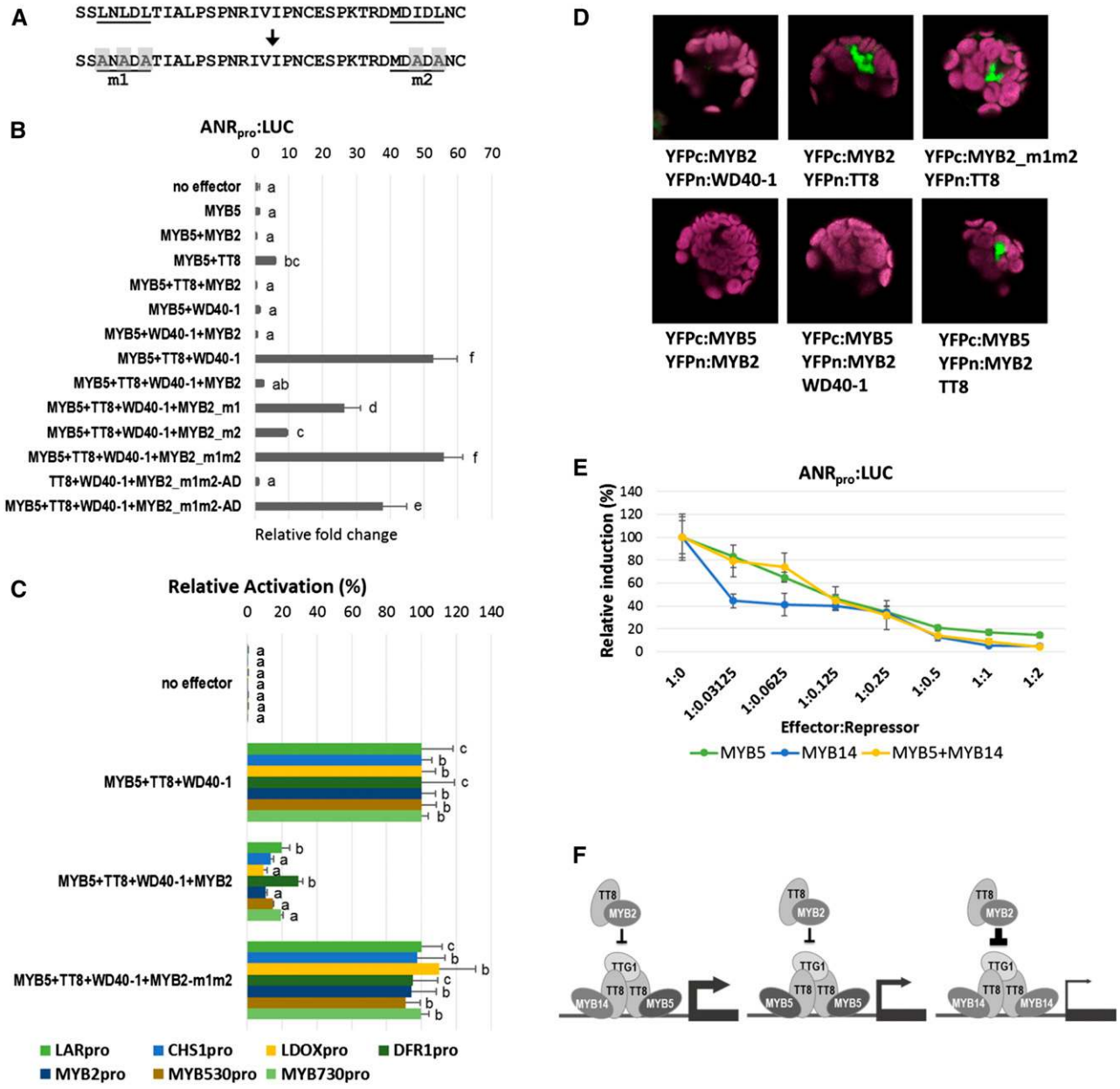

Figure 4. Regulatory Mechanism of MYB2 on Target Promoters.

(A) Analysis of repression motifs of MYB2 protein. The conserved and semiconserved EAR motifs are underlined and the five amino acids changed to Ala are indicated by shadow in two modified versions of the MYB2 protein (m1 and m2).

(B) Activation and repression of the *ANR* promoter in transient expression assay using Arabidopsis protoplasts. Various combinations of *M. truncatula* effectors (MYB5, TT8, WD40-1, MYB2, MYB2_m1, MYB2_m2, MYB2_m1m2, and MYB2_m1m2-AD) were used to transfect Arabidopsis protoplasts along with the *ANR* promoter fused with luciferase reporter. Data are means ± SD (*n* = 3 biological replicates). Significant difference was determined by one-way ANOVA (LSD, P = 0.05) and indicated by letters.

(C) Activation and repression assays of the various target promoters. Data are means ± SD (*n* = 3 biological replicates). Significant difference for each promoter was determined by one-way ANOVA (LSD, P = 0.05) and indicated by letters.

(D) BiFC assay showing the physical interaction between MYB2 and TT8 or MYB5 (TT8-mediated). eYFP signals are localized in the nucleus and are shown in green and chloroplast autofluorescence is shown as magenta.

(E) Dosage-dependent suppression of MBW complex activities by MYB2. Serial dilutions of the MYB2 construct were cotransfected with different effector combinations (MYB14-TT8-WD40-1, MYB5-TT8-WD40-1, and MYB5-MYB14-TT8-WD40-1). Data are means ± SD (*n* = 3 biological replicates).

filled with green staining, and smaller vacuoles or vesicle structures that had weak TBO staining were detected in the upper side of the cells in both R108 and *myb2* mutant plants (Supplemental Figures 15B, 15B-III, 15C, 15E, 15E-III, and 15F). In the chalaza, enlarged multiple vacuoles with green staining were found in multiple or closely packed macrosclereids (Supplemental Figures 15B, 15B-II, 15C, 15E, 15E-II, and 15F). However, there was no indication of PA accumulation or PA-vacuole formation in the epidermal layer of the distal side of the seed coat (Supplemental Figures 15B, 15B-IV, 15E, and 15E-IV). We also could not observe PA staining in hypodermal cells (osteosclereid precursors) and inner parenchyma cells throughout the entire seed coat, except the mycropylar-chalazal extension region where the seed coat is more enlarged. In this region, the staining was expanded to a group of round parenchyma cells close to vascular bundles, and small prevacuolar structures containing PA were found inside or outside of the central vacuole (Supplemental Figures 15B, 15B-I, 15C, 15E, 15E-I, and 15F).

In the *wd40-1* mutant, the staining in the epidermal layer completely disappeared, confirming that the TBO staining in the same cell files of both wild-type and *myb2* seeds was indeed PA deposition (Supplemental Figures 15G, 15H, 15H-I to 15H-IV, and 15I). Green TBO staining was only detected in the xylem tissue of chalazal vessels in *wd40-1* seed (Supplemental Figure 16).

To compare the proximal-distal seed axis at the same longitudinal position, transverse sections of 10 DAP wild-type and *myb2-1* (NF10162) mutant seeds were made. In the section across the developing cotyledon, PA in the large vacuole was more densely stained on the hilar side of *myb2* seeds, although the vacuolar size was similar to that of the wild type (Supplemental Figures 17B, 17B-I, 17D, and 17D-I). In the middle section dissecting the hilum, only the *myb2* mutant had faint green staining in the small vacuolar structures of epidermal cells at the boundary of the proximal and distal region (Supplemental Figures 18B, 18B-III, 18D, and 18D-III). There was no sign of PA accumulation on the distal side of the seed body in either wild-type or *myb2* mutant seeds (Supplemental Figures 17B, 17B-III, 17D, 17D-III, 18B, 18B-IV, 18D, and 18D-IV). In the *wd40-1* mutant, the generation of an empty vacuole of normal size in the epidermal layer was more obvious in the transverse sections (Supplemental Figures 17E, 17F, 17F-I to 17F-III, 18E, 18F, and 18F-I to 18F-IV).

To examine differences in spatial patterns of PA accumulation at a more mature stage, transverse sections of wild-type R108, *myb2-1* (NF10162), and *wd40-1* were compared at 12 DAP (bent cotyledon stage). On the proximal side of the upper region across the hypocotyl of the developing embryo, the vacuoles containing PA in the epidermis were enlarged and occupied almost half of the cytoplasm, with bright green TBO staining compared with 10 DAP seeds (Figures 5B, 5B-I, 5D, and 5D-I). In parenchyma cells of the middle region, the small vacuoles remained as aggregated but still separate granular structures (Figures 5H, 5H-I, 5J, and 5J-I). The PA staining sometimes appeared to be diffused in the entire central vacuole but with stronger staining near the tonoplast (Figures 5H, 5H-I, 5J, and 5J-I). The most distinct difference in spatial distribution of PAs between the wild type and *myb2* mutant at this stage was detected in the boundary between the proximal and distal axis. The epidermal cells of *myb2* had vacuoles positioned at both ends of the cells that stained densely with TBO (Figures 5D, 5D-III, 5J, and 5J-III). In the wild-type seeds, only some of the vacuoles were weakly stained with green color in the upper section and no staining was found in the middle area (Figures 5B, 5B-III, 5H, and 5H-III). Although the sizes of the cell files were smaller and the cytoplasmic staining was denser, small vacuoles with weak TBO staining were seen in the *myb2* mutant even on the distal side of the seed (Figures 5D, 5D-IV, 5J, and 5J-IV). These data indicate that PA accumulation in the vacuole or vesicle is proceeding in the seed body of the *myb2* mutant even though the differentiation of the cell file based on cell elongation, vacuole formation, and cuticle accumulation has progressed to the same phase as in the wild type. In the *wd40-1* mutant, the cell file developed as normal but the vacuole was empty and there was no staining detected with TBO (Figures 5E, 5F, 5F-I to 5F-IV, 5K, 5L, and 5L-I to 5L-IV). The development of cuticle was not affected in *myb2* or *wd40-1* seeds compared with the wild type at both 10 and 12 DAP (Figure 5; Supplemental Figures 15, 17, and 18). We could not obtain TBO staining data for older seeds due to the limitation of permeability of fixative and resin.

To confirm that the blue-green TBO staining in the epidermal layer represents PAs and/or PA precursors, 12 DAP seeds were sectioned after DMACA staining (Figure 6). In the longitudinal sections, strong purple staining with DMACA was colocalized with TBO staining in macrosclereids and some parenchyma cells around the hilum area in both R108 and *myb2-1* (NF10162) mutant seeds. The coloration was more expanded in the epidermal layer of *myb2* seeds (Figures 6A and 6B). The same expansion was also observed in transverse sections across the upper side of the seeds (Figures 6E and 6F). DMACA staining was dispersed in the entire epidermal layer rather than being restricted to the vacuole, but it appeared most intense near the tonoplast, and strong purple aggregations attached to the vacuolar membrane were observed in DMACA-positive cells (Figures 6E, 6E-I, 6F, and 6F-I). Weak purple staining was continuous to the seed body only in *myb2* mutants (Figures 6E, 6E-II, 6F, and 6F-II). There was a complete absence of DMACA staining in *wd40-1* seeds (Figures 6C, 6G, 6G-I, and 6G-II). In mutant *myb14-1* seeds, DMACA staining disappeared in the epidermal cells in the hilum groove and in parenchyma cells. The weak staining in other areas compared with the wild type is possibly due to the redundancy of Mt MYB14 with the other MYB transcription factors PAR or Mt MYB5 (Figures 6D, 6H, 6H-I, and 6H-II).

MYB2 Represses *ANR* in the *M. truncatula* Seed Coat

Given that ANR is a key enzyme specific for PA biosynthesis in the seed coat and is an immediate target of the MBW complex and

Figure 4. (continued).

(F) Putative mechanism of MYB2 and MYB5/MYB14 MBW activator complexes to differentially regulate the promoter activity of a target gene. MYB2 interaction with MYB5/MYB14 MBW activator complexes is mediated by TT8. MYB2-TT8 dimer may bind to the complex or replace one of the activator MYBs with MYB2, leading to suppression of transcription in a dosage dependent manner.

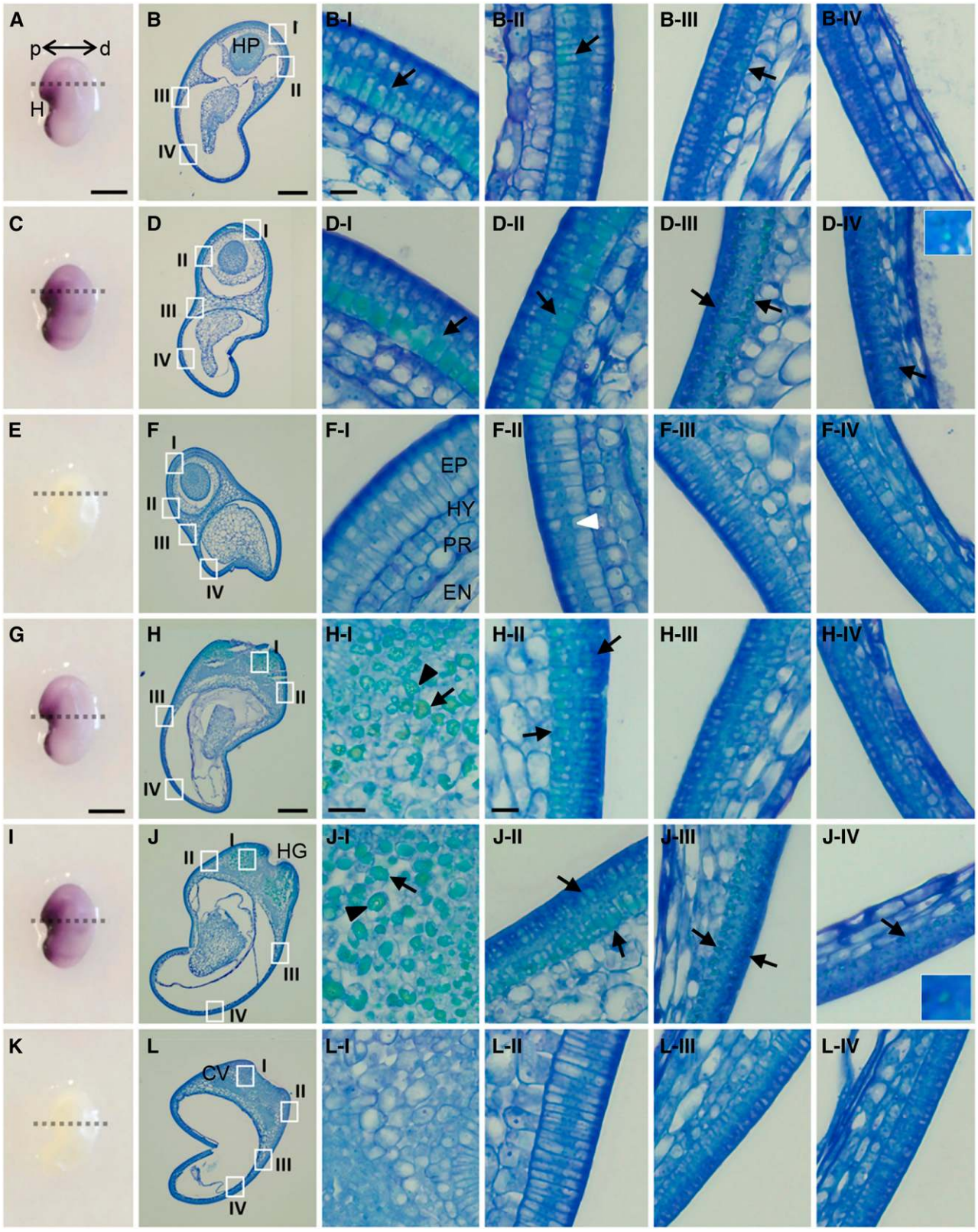

Figure 5. Regulation of Progressive PA Deposition in the *M. truncatula* Seed Coat by MYB2.

MYB2, we compared the *ANR* expression pattern in wild-type and *myb2* mutant seeds to determine where MYB2 protein suppresses *ANR* expression in vivo. In young wild-type seeds, an ANR_{pro}*:GUS* construct was strongly expressed in the hilar area, although weak GUS activity was detected in the entire seed coat (Figure 7A). In the hilar area, strong *ANR* expression was diffused into parenchyma cells, which normally accumulate PA (Figures 7A, 7E, and 7I). In the seed body beside the hilar region, weak GUS activity was only detected in the epidermal layer of the seed coat in developing seeds (Figures 7E and 7F). In the *myb2* mutant background, strong *ANR* expression was detected in the outside of the hilar area, and GUS activity was more evenly distributed in the entire seed coat (Figure 7B). However, the expression still appeared to be strongest in the outermost cell layer (Figures 7J and 7K). These results are consistent with the expanded regions of PA accumulation in the *myb2* mutant seeds.

Additionally, we examined the activity of a $MYB2_{pro}$*:GUS* reporter gene construct in *M. truncatula* seed and found that *MYB2* expression was excluded from the hilar region (Figures 7C, 7D, 7G, and 7M), conversely to PA accumulation and *ANR* expression. *MYB2* expression was strong in the seed body but became faint as seeds matured (Figures 7C and 7D), which is consistent with the microarray data. *MYB2* promoter activity was strongest in the epidermal layer circumventing the seed body and was more diffused into inner cell files, including the endosperm in the distal region of the seed body (Figures 7G, 7H, and 7M to 7O). Faint GUS activity was also detected in the parenchyma cell files close to chalazal vessel branches (Figure 7M). Overall, these expression analyses indicate that MYB2 represses PA accumulation in the seed body by suppressing *ANR* expression at the early stage of seed development.

We also checked $MYB2_{pro}$*:GUS* activity in other tissues, including flower and seedling, which exhibit ectopic anthocyanin accumulation in the *myb2* mutant. *MYB2* expression was detected in the hypocotyl and in the junction between the hypocotyl and root of 7-d-old seedlings (Figure 7L). *MYB2* was also expressed in the middle of the banner of the flower, making a semicircle with stronger GUS staining at the periphery (Figure 7P). In the strongest expression line analyzed, GUS activity in the flower was more diffused into the center of the banner and in the base of the wing and keel petals (Supplemental Figure 19A). GUS activity was detected in the cotyledon and root, where strongest staining was observed in the vasculature and lateral root tips (Figure 7L; Supplemental Figure 19B). In the shoot apex, promoter activity was specifically localized in the trichomes of the inflorescence meristem, young flowers, and leaves, with more diffused expression at wounding sites (Supplemental Figures 19C and 19D). Relatively strong *MYB2* expression was detected in the developing pod and its trichomes (Supplemental Figures 19E and 19F). We also observed GUS staining in the tip of the style, anther, and ovary (Supplemental Figure 19A).

DISCUSSION

MYB2 Is a Repressor of Both Anthocyanin and PA Biosynthesis

Although the timing of accumulation and spatial distribution of anthocyanin and PA has been investigated in several plant species, information on the components involved in fine-tuning the progression of pigmentation is still limited. Recently it has been shown that regulatory circuits including an MBW complex and a repressor have been adopted for the regulation of flavonoid biosynthesis through the study of Arabidopsis MYBL2 and petunia MYB27 and MYBx. Here, we presented a detailed spatial and temporal analysis of accumulation of PAs during *M. truncatula* seed development and found that MYB2, an R2R3 MYB repressor, plays a key role in regulating the progression of PA accumulation, in addition to regulating anthocyanin pigmentation in seedling and flower.

MYB2 is classified in the MYB TF subgroup 4 along with MYB4-like proteins, from *M. truncatula* and other organisms, which have complete R2R3 domains and a diagnostic C1 motif (Shen et al., 2012). However, in phylogenetic analyses with either the R2R3 or R3 domain (for S-MYB) sequence or the entire protein sequence, a group of proteins including Mt MYB2, Ph MYB27, Ptr MYB182, and Vv MYBC2s are separated from the MYB4 lignin/phenylpropanoid MYBs. Among the proteins belonging to the Fa MYB1-like group and MYBL2, some have been identified as anthocyanin repressors and others are known as both anthocyanin and PA regulators through overexpression analysis. However, the N-terminal domains of these proteins appear to be highly conserved, and no clear distinction of protein sequence or specific amino acid

Figure 5. (continued).

(A), **(C)**, and **(E)** DMACA-stained seeds of wild-type, *myb2-1* (NF10162), and *wd40-1* plants at 12 DAP.
(G), **(I)**, and **(K)** DMACA-stained seeds of wild-type, *myb2-1* (NF10162), and *wd40-1* plants at 12 DAP.
(B) and **(H)** Transverse section of R108 seeds at 12 DAP stained with TBO.
(D) and **(J)** Transverse section of *myb2-1* (NF10162) seeds at 12 DAP stained with TBO.
(F) and **(L)** Transverse section of *wd40-1* seeds at 12 DAP stained with TBO.
At 12 DAP (bent cotyledon stage of embryo), progressive differentiation of the cell files from proximal (p) to distal (d) axis was observed. A thick cuticle layer on the outer surface of the hilar side indicated that the proximal side was more differentiated compared with the distal side, where small cells with dense cytoplasm were observed. The magnified views of the regions boxed in **(B)**, **(D)**, **(F)**, **(H)**, **(J)**, and **(L)** are denoted by I, II, III, and IV. Double-headed arrow indicates the proximal-distal axis. Dashed lines indicate the position of the cross section. White arrowhead indicates the nucleus containing nucleolus aligned in the middle of the macrosclereid cells. Black arrowheads denote the PA-positive central vacuole with granule structures of small vacuoles. Arrows indicate the vacuole with accumulation of PAs or PA precursors. Magnified views of PA-containing vacuole are shown in the boxes in **(D-IV)** and **(J-IV)**. CV, chalazal vessel; EN, endosperm; EP, epidermis; H, hilum; HG, hilar groove; HP, hypocotyl of embryo; HY, hypodermis; PR, parenchyma. Bars = 1 mm in **(A)**, **(C)**, **(E)**, **(G)**, **(I)**, and **(K)**, 0.25 mm in **(B)**, **(D)**, **(F)**, **(H)**, **(J)**, and **(L)**, 10 μm in **(B-I)** to **(B-IV)**, **(D-I)** to **(D-IV)**, **(F-I)** to **(F-IV)**, **(H-II)** to **(H-IV)**, **(J-II)** to **(J-IV)**, and **(L-II)** to **(L-IV)**, and 10 μm in **(H-I)**, **(J-I)**, and **(L-I)**.

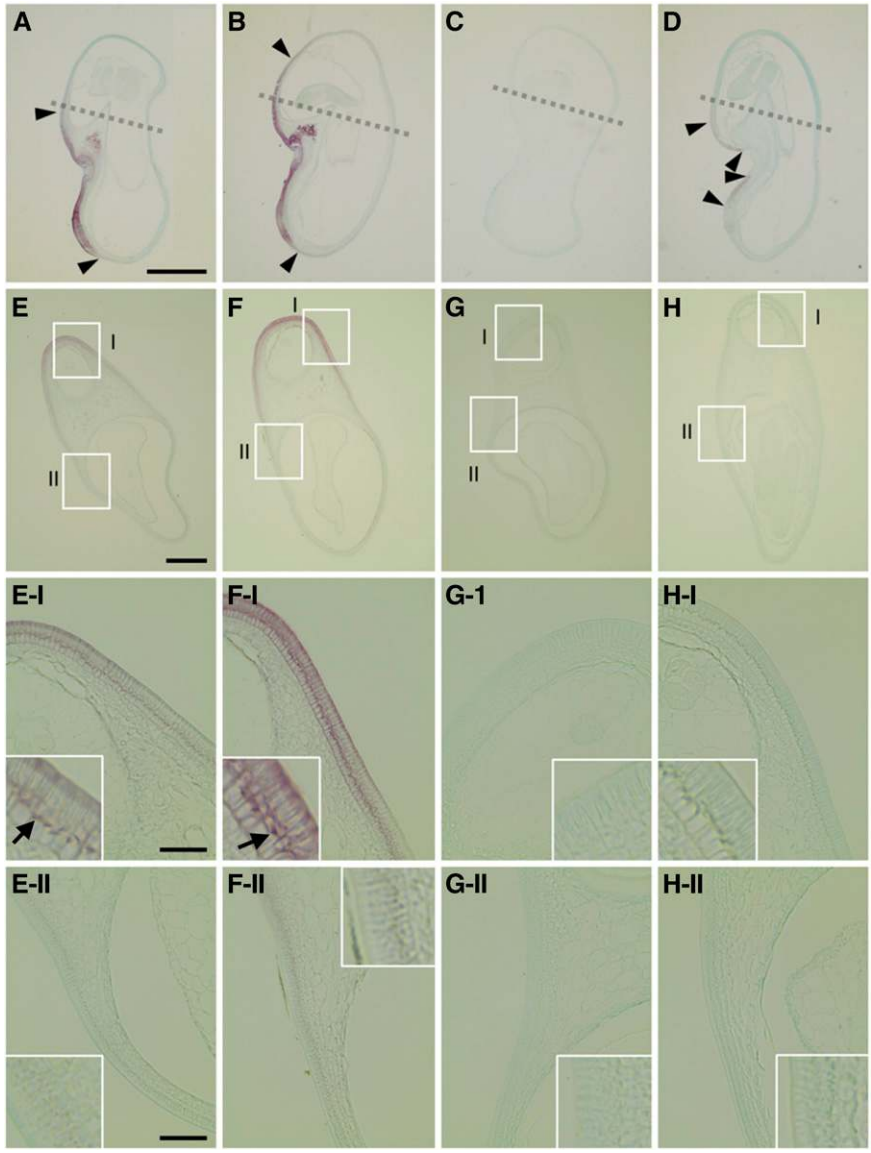

Figure 6. DMACA Staining of PA Accumulation in *M. truncatula* Seeds.

(A) Longitudinal section of R108 seeds at 12 DAP.
(B) Longitudinal section of *myb2-1* (NF10162) seeds at 12 DAP.
(C) Longitudinal section of *wd40-1* seeds at 12 DAP.
(D) Longitudinal section of *myb14-1* seeds at 12 DAP.
(E) Transverse section of R108 seeds at 12 DAP.
(F) Transverse section of *myb2-1* (NF10162) seeds at 12 DAP.
(G) Transverse section of *wd40-1* seeds at 12 DAP.
(H) Transverse section of *myb14-1* seeds at 12 DAP.

Wild-type (R108), *myb2-1*, *wd40-1*, and *myb14-1* seeds at 12 DAP were stained with 0.5% DMACA in absolute ethanol containing 0.8% w/v HCl and used for sectioning. The magnified views of the regions boxed in **(E)** to **(H)** are denoted by I and II. Dashed lines indicate the position of the cross section. The magnified view of the epidermal layer is shown in the boxes in **(E-I)**, **(E-II)**, **(F-I)**, **(F-II)**, **(G-I)**, **(G-II)**, **(H-I)**, and **(H-II)**. Arrowheads indicate the end points of DMACA-stained cells in the epidermal layer and arrows denote intense PA coloration with DMACA near the tonoplast. Bars = 0.25 mm in **(A)** to **(D)**, 0.25 mm in **(E)** to **(H)**, and 50 μm in **(E-I)**, **(E-II)**, **(F-I)**, **(F-II)**, **(G-I)**, **(G-II)**, **(H-I)**, and **(H-II)**.

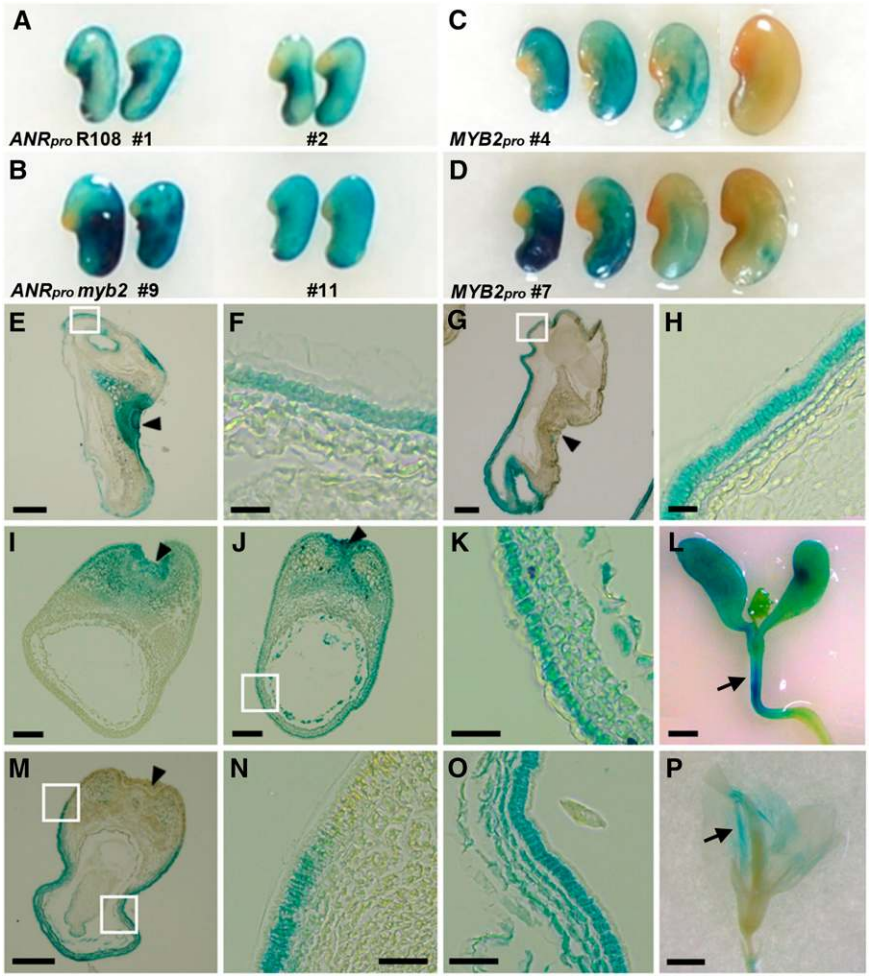

Figure 7. Regulation of *ANR* Expression by MYB2.

(A) Representative expression patterns of ANR_{pro}*:GUS* construct in two independent transgenic lines of wild-type R108 background.
(B) Representative expression patterns of ANR_{pro}*:GUS* construct in two independent transgenic lines of *myb2* mutant background.
(C) and **(D)** Representative expression patterns of $MYB2_{pro}$*:GUS* construct in two independent transgenic lines of *M. truncatula* R108.
(E) and **(F)** Longitudinal section of ANR_{pro}*:GUS* R108 seed.
(G) and **(H)** Longitudinal section of $MYB2_{pro}$*:GUS* R108 seed.
(I) Transverse section of ANR_{pro}*:GUS* R108 seed.
(J) and **(K)** Transverse section of ANR_{pro}*:GUS myb2* seed.
(M) to **(O)** Transverse section of $MYB2_{pro}$*:GUS* R108 seed.
(L) and **(P)** Representative expression patterns of $MYB2_{pro}$*:GUS* construct in seedling and flower.
Arrows indicate hypocotyl and the center of banner petal, which have ectopic anthocyanin accumulation in *myb2* mutant. Arrowheads indicate hilum. **(F)**, **(H)**, **(K)**, and **(N)** and **(O)** are the magnified views of the regions boxed in **(E)**, **(G)**, **(J)**, and **(M)**, respectively. Bars = 1 mm in **(L)** and **(P)**, 0.5 mm in **(G)**, 0.2 mm in **(E)** and **(M)**, 0.1 mm in **(I)** and **(J)**, 50 μm in **(H)** and **(K)**, 25 μm in **(N)** and **(O)**, and 10 μm in **(F)**.

changes are found between these two classes as have been reported in comparisons between anthocyanin and PA activators (Supplemental Figure 5; Heppel et al., 2013).

MYB2 has a canonical EAR motif sequence, and mutation of the three Leu residues in this motif to Ala only partially compromised the repressive activity of MYB2 and did not inhibit its interaction with TT8. Only additional mutation at the C-terminal end (semiconservative EAR motif) fully abolished MYB2's ability to suppress transcriptional activation activity of the MBW complex. Approximately 25% of currently described EAR motif-containing proteins are known to have more than two EAR motif sites (Kagale et al., 2010). Although the biological and evolutionary significance of amplification of the EAR motif in a single protein has not been systematically analyzed, it is possible that it strengthens the mechanism of repression, or different motifs in a different sequence context in the region surrounding the EAR motif may influence the ability of the protein to interact with different corepressors or other potential interactors, given the protein-protein interactions known for EAR motif-containing proteins (Hill et al., 2008). All of these considerations suggest that the functional specification of MYB2 as an anthocyanin or PA repressor is

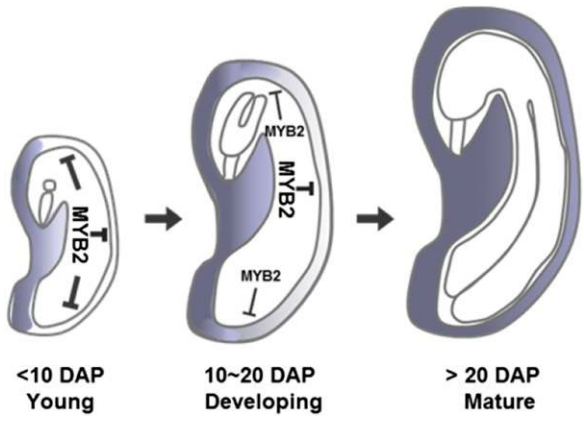

Figure 8. Model for Regulation of PA Accumulation by MYB2 in the *M. truncatula* Seed Coat.

PA accumulation initiates from the epidermis and parenchyma cells in the hilar area at the early stage of seed development and gradually expands to the seed body. This process is controlled by MYB2 acting as a negative regulator of MYB5/MYB14 MBW complexes. The signal for the repression of *MYB2* may be generated from the hilar area and transmitted to the seed body, resulting in progressive suppression of *MYB2* expression to inversely induce *ANR* transcription and PA accumulation in the entire seed coat.

dependent on the cellular context in which the specific MBW complex is functional at a specific time and in a specific tissue.

The expression data show that MYB2 plays a role in regulation of most anthocyanin and PA pathway genes since both common and specific pathway genes are upregulated, which is consistent with the increase in both anthocyanin and PA contents in *myb2* mutant plants. Accordingly, *MYB2* expression appears to be strong in the region where PAs and/or anthocyanins are ectopically accumulated in the *myb2* mutant compared with the wild type. However, we only saw minor changes in target gene expression in *myb2* seed at 12 DAP, possibly due to the fact that a large proportion of the PAs are accumulated in the hilum area, which already has an intense and broad expression domain in the wild type. During *M. truncatula* seed development, the soluble PA content becomes reduced while insoluble PA levels increase due to secondary changes in PA to form an oxidized complex with polysaccharides and other cellular material. Even though it gradually decreases during the development of both wild-type and *myb2* seed, the soluble PA amount in the *myb2* mutant is always higher than in the wild type, indicating that MYB2 is involved in the regulation of PA quantity as well as the progression of PA accumulation. The higher content of insoluble (nonextractable) PA in 16, 20, and 30 DAP mutant seeds indicates that the secondary changes in PA quality are accelerated as a result of loss of function of MYB2. This may be partially due to increased PA monomer and polymer generation, but it is possible that the secondary processes are also deregulated in *myb2* seeds.

Regulatory Network of MYB2 and MBW Activator Complexes

Arabidopsis MYBL2 interacts with TT8, and Ph MYB27 can make a complex with DPL (an R2R3-MYB) when JAF3 or AN1 bHLH proteins are provided in a yeast three-hybrid assay (Matsui et al., 2008; Albert et al., 2014). In our experiments, the repression activity of MYB2 is highest when TT8 is coexpressed in transient assays. In addition to direct interaction between MYB2 and TT8, we also observed that interaction of MYB2 with MYB5 or MYB14 is mediated by TT8 in BiFC experiments. The mutant version (MYB2_m1m2) of MYB2 still interacts with TT8 but has no titration effect in transient assays, indicating that passive competition is not the major regulatory mechanism for the inactivation and suggesting that MYB2 functions as an active repressor via TT8-mediated direct contact with MBW complexes on the target promoter. Although MYB2 has conserved R2R3 domain sequences for DNA binding, it is not clear whether MYB2 binds to the promoters of target genes, and dimerization of TT8 through its ACT C-terminal region or bHLH domain can generate a MYB2 repressor complex in cells lacking activator MYB proteins.

In a previous report, we showed that MYB5 and MYB14 are able to activate the *ANR* promoter synergistically and that MYB5 and MYB14 form the complex in a TT8- and WD40-1-dependent manner (Liu et al., 2014). MYB5 or MYB14/MYB5 complexes on the *ANR* promoter are more resistant to MYB2 inhibition than the MYB14 MBW complex when MYB2 protein level is relatively low. This suggests that MYB5 plays a role in stabilizing the MBW complex, possibly by a conformational change of the quaternary complex, in addition to functioning as a transcriptional activator. This could represent a mechanism to initiate or maintain high expression of target genes when both MYB14 and MYB5 are expressed without being affected severely by repressors such as MYB2.

In the *myb2* mutant, expression of regulatory components is also changed. In addition to TT8, we found that *MYB530*, the closest homolog of MYB2, and *MYB730* (R3 MYB) are also induced in seedlings and seeds of *myb2* mutants. Also, the promoters of *MYB2*, *MYB530*, and *MYB730* are regulated by the MBW complex and MYB2 in transient assays, indicating that they are directed by a feedback regulatory network.

Multidimensional networks of transcriptional activation and repression are known to underlie responses to stress or hormones in plants (Kazan, 2006; Voß et al., 2014). The dynamic response of negative feedback loops seems to be used to maintain homeostasis at the cellular or tissue level. Thus, the antagonistic mechanism incorporating MBW activator complexes and multiple negative regulators may facilitate the fine tuning of flavonoid biosynthesis and protect plants from accumulation of excessive and potentially toxic levels of PAs, anthocyanins, or their precursors. Ectopic anthocyanin biosynthesis in *myb2* seedlings suggests that MYB2 expression or activity may be repressed under circumstances such as high-light treatment or nutrient deprivation, leading to stress-induced anthocyanin accumulation. In this respect, it has been reported that Arabidopsis *MYBL2* and petunia *MYB27* and *MYBx* expression is altered by different light conditions (Dubos et al., 2008; Albert et al., 2014). Although it is known that MYBL2 protein is stabilized by BRASSIONSTEROID-INSENSITIVE 2 (BIN2), which negatively regulates the brassinosteroid (BR) pathway, it is not clear how *MYBL2* and *MYB27* expression is suppressed under high-light treatment. It is also interesting that *MYB2* expression is almost completely excluded from the strong *ANR* expression and PA accumulation sites, which are possible

MYB5 and *MYB14* expression domains, but is induced in the seed body of developing seeds. MYBL2 regulation by BR suggests that MYBL2 functions as a mediator to link hormone response and flavonoid biosynthesis (Ye et al., 2012). In this respect, it remains to be determined whether the regulation of *MYB2* transcription or post-transcriptional regulation of MYB2 activity or stability are mediated by hormones such as GA, which are known to orchestrate seed coat differentiation.

Cellular and Subcellular PA Accumulation in the *M. truncatula* Seed Coat

There is a distinct difference in PA pigmentation pattern in the seeds between Arabidopsis and *M. truncatula*. PAs are accumulated in endothelium, chalazal pigment strand, and micropylar cells derived from inner integument layers in Arabidopsis, whereas they are mainly synthesized, in a progressive manner, in the outermost layer of the seed coat derived from the outer integument in *M. truncatula*. Arabidopsis epidermal cells produce and secrete a large quantity of mucilage outside of the seed coat. Thus, the epidermal layer is committed to mucilage accumulation, and PA biosynthesis is localized in endothelial cells. In contrast, in *M. truncatula* and other legume seeds, rigidity and impermeability of the seed coat seems to be more dependent on PA production in its epidermal layer, since these cells shows extensive cell wall thickening, with cuticle aligned outside, instead of mucilage production. In fact, in several legumes, seed coat pigmentation is known to correlate with impermeability and seed dormancy (Smýkal et al., 2014).

Previously, the promoter activity of *BAN* (*ANR*) was found to be initiated from micropyle to chalaza and terminated in the seed body in Arabidopsis. This suggests possible repression of a negative regulator induced by fertilization in the micropyle or chalaza but not in the seed body. Our data show similar accumulation of PA in *M. truncatula* in the hilar area and chalazal and micropyle extension domains at the early stage of seed development and expansion of pigmentation to the seed body later. Consistently, *ANR* expression was found to be strong in the hilar area, and complete suppression of $MYB2_{pro}$*:GUS* activity was observed in the same area. This suggests that the signal for repression of *MYB2* is generated from the hilar area and would be transmitted by diffusion or cell-to-cell signaling to the seed body, resulting in progressive suppression of *MYB2* expression to inversely allow for PA accumulation (Figure 8).

The demarcation of the PA accumulation domain in the early stage of seed coat development and the complex positive and negative regulators involved in the process reflect pattern formation and cell specification found in Arabidopsis trichome and root hair development. Given the fact that epidermal pattern formation is determined by MBW complexes and their associated repressors (Schiefelbein, 2003), the basic antagonistic mechanism underlying epidermal cell differentiation is conserved in different organs (root, shoot, and seed) and operates through the same set of regulators in plants. In particular, it will be interesting to determine how the function of other potential negative regulators, such as *M. truncatula* MYB530 and MYB730, are incorporated and coordinated to refine gradual PA accumulation in the seed coat and optimize the level of PA biosynthesis.

In cross sections of the *M. truncatula* seed coat, PA-containing vacuoles are detected from both ends of the cells at the early stage of epidermal cell differentiation. Later they appear as a single vacuole in cells at the opposite side of the seed surface in the epidermal layer. In the parenchyma cells around chalazal vessels, small provacuolar structures (or vesicles) appear to be isolated but most are attached to the central vacuole or collate inside the vacuoles. These data support a model in which PA precursors are transported through ER-derived vesicles to the vacuole rather than the assumption that the uptake of PA precursors into endomembranes takes place at the level of the vacuole rather than the ER, based on the distribution of the TT12 and MATE1 transport proteins. Previous reports showed that PA storage was confined to prevacuole-like small vesicles, without generation of a central vacuole, in the Arabidopsis *tds4*, *tt19*, and *tt12* mutants (Abrahams et al., 2003; Kitamura et al., 2010), and a similar phenotype and developmental delay of the PA-containing central vacuole was reported in the *aha10* proton pump mutant (Baxter et al., 2005). On the basis of these observations, it has been suggested that PA accumulation and vacuole biogenesis are linked (Baxter et al., 2005). However, cross sections of *wd40-1* mutant seeds clearly show that vacuole formation and enlargement is not linked to PA or flavonoid biosynthesis in the seed coat. *wd40-1* seeds develop a vacuole as large as the wild type, and more PA accumulation does not affect the size of the vacuole and timing of vacuole generation in the *myb2* mutant, meaning that PA-containing vacuole is not the end product of small vesicle fusion, at least in the seed coat. Thus, the central vacuole phenotypes detected in some *tt* mutants may result from accumulation of toxic upstream intermediates that delay or interrupt vacuole biogenesis. Since unbound PA staining is never observed, it is possible that MATE1 or transport-related proteins comigrate with flavonoids (conjugates) or intermediates in trafficking vesicles to load them into the vesicle rather than the vacuole, and it will be interesting to determine whether PA sequestration in the vacuole is mediated by structures such as anthocyanin vacuolar inclusions (with no membrane envelope) or prevacuolar compartments, as shown for anthocyanins (Zhang et al., 2006; Poustka et al., 2007).

The growth and differentiation of ovular integuments to produce a complex structure is the most dramatic cellular change in seed development and is critical to protect the embryo and maintain its growth. Early embryo development and differentiation are known to be regulated by surrounding maternal tissue, and transmission of signaling molecules and nutrient from the mother plant is mediated by the seed coat. One of the major functions of the legume seed coat is the lateral transfer of assimilates and other nutrients before they are released to the developing embryo. Since the *M. truncatula* seed coat has a relatively simple vascular system that consists of a single chalazal vascular bundle and two short branches, nutrient transfer via the symplastic pathway or passive apoplastic movement through the seed coat could be critical for the early stage of seed development. Thus, progressive epidermal cell differentiation and PA accumulation in the seed body could be a mechanism to maintain functional cell files for nutrient transport and storage in the seed coat before embryo development is finished and to coordinate further seed filling and desiccation processes. However, high PA accumulation in the hilar area from the early stage of seed development suggests that PAs are used to

reduce water loss and to protect seeds from pathogen ingress. Later, abundant PA accumulation and oxidation in macrosclereids contributes to water impermeability and rigidity of the seed coat (hardseededness) in addition to cuticle formation. In common bean (*Phaseolus vulgaris*), PA starts to accumulate in the seed coat tissue nearest the hilum (Bassett and Miklas, 2007), and the i^i allele of *I* (Inhibitor) locus in soybean (*Glycine max*) results in pigmentation only in the hilum (Tuteja et al., 2004). Thus, this contrasting cellular status associated with different functional requirements (nutrient transport and metabolism to support embryogenesis vs. physical and structural barrier to guarantee protection) should be balanced during seed development.

So far, no developmental defects of embryo or seed structure have been observed in most PA defective mutants, including *myb2*, and genetic ablation of the endothelial cell layer in Arabidopsis resulted in only slightly reduced seed dormancy. In *myb2* mutants, ectopic PA accumulation was only detected in the outermost cell layer and strong *ANR* expression was still mainly confined to the epidermal layer even though *MYB2* expression was more diffused into inner layers of the seed body, indicating that epidermal layer-specific control mainly given by the MBW complex should be tightly regulated to avoid potential damage due to PA accumulation in nonspecialized cells. Alternatively, weak expression of *ANR* in other layers in the *myb2* mutant may not be sufficient to support PA accumulation possibly due to limited supply of other enzymes or precursors. Better understanding of the regulatory mechanisms underlying PA accumulation in the seed coat will illuminate the crosstalk between the flavonoid pathway and other developmental and physiological pathways in plants.

METHODS

Plant Materials

Medicago truncatula ecotype R108 was used as the wild type for comparison with *Tnt1* insertion mutants. The tobacco (*Nicotiana tabacum*) *Tnt1* insertion-mutagenized *M. truncatula* population was screened to identify *myb2-1* (NF10162) and *myb2-2* (NF19285) mutants as described previously (Tadege et al., 2008). Seeds were scarified with concentrated sulfuric acid for 10 min and then washed four times with water. Scarified seeds were sterilized with 30% bleach for 4 min and then rinsed three times with sterile water. Sterilized seeds were vernalized at 4°C for 5 d and germinated for 5 d on half-strength B5 medium before transfer to soil. The plants were grown in a greenhouse set at 16-h/8-h day/night cycle at 24°C. Murashige and Skoog medium containing 0.5% sucrose was used for the analysis of seedling phenotypes.

Plasmid Constructions for Generating *MYB2*-Overexpressing Plants

To generate binary vectors for *MYB2* overexpression, the cDNA sequence was amplified by RT-PCR from seed RNA using the primer pairs MYB2-F/MYB2-R (Supplemental Table 1 for all oligonucleotide primers used in this work). Amplified cDNA was first cloned into pENTRD vector and then cloned into pB7GW2D binary vector containing the CaMV 35S promoter by LR recombination reaction to generate Mt MYB2-pB7GW2D binary vector. A *GUS* gene was used to construct GUS-pB7GW2D binary vector as control. The binary vector was transformed into *Agrobacterium rhizogenes* strain ARqua1 and transformed colonies were used to inoculate radicles of *M. truncatula* (cv Jemalong A17) seedlings as described previously in the Medicago Handbook at http://www.noble.org/Global/medicagohandbook/pdf/AgrobacteriumRhizogenes.pdf. The resulting hairy roots were maintained on B5 medium.

RNA Isolation, qRT-PCR, and DNA Microarray Analysis

RNAs from plant tissues were isolated using Plant RNA Reagent (Invitrogen). Isolated RNAs were treated with DNase I and then purified by RNeasy MinElute Cleanup Kit (Qiagen). Cleaned RNAs were used to perform reverse transcription with SuperScript III reverse transcriptase (Invitrogen). qRT-PCR analysis with Power SYBR Green PCR Master Mix (Life Technologies) was confirmed with three biological replicates and performed on an QuantStudio 6 Flex Real-Time PCR system (Life Technologies) according to the manufacturer's instructions. Two (for seeds) and three (for hairy roots) biological replicates were used for microarray analyses using the *M. truncatula* GeneChip (Affymetrix) according to the manufacturer's instructions. Raw data were normalized by the robust multichip averaging method. Presence and absence calls for probe sets were obtained using the dCHIP algorithm (Li and Wong, 2001). Type I family-wise error rate was calculated using a Bonferroni-corrected P value (threshold 0.05). To identify differentially regulated probe sets, we used a P value threshold of 5% and at least a 2-fold difference between transformant/mutant lines and their respective controls.

Quantification of PAs

Plant materials were first ground to a powder in liquid nitrogen, and ~100 mg of materials was used for extraction. Extraction was performed three times with 1 mL 70% acetone and 0.5% acetic acid, as described (Pang et al., 2008). Assay of soluble PAs (with DMACA reagent) and insoluble PAs (with butanol-HCl) was performed as described previously (Pang et al., 2008). Determination of PA composition by normal and reverse-phase HPLC analyses, including size estimation by HPLC followed by postcolumn derivatization with DMACA, and phloroglucinolysis, were performed as described by Pang et al. (2008).

Microscopy

Cross-sectioning of developing seeds was performed as described previously (Debeaujon et al., 2003) with the following modifications. The 8-μm sections were made on an RM 2245 microtome (Leica Microsystems) and stained for 30 s in 0.1% (w/v) TBO (Research Organics) in 0.1 M phosphate buffer, pH 7.2. The TBO stain develops a greenish-blue color when associated with polyphenolic compounds such as PAs and lignins. It also stains pectic substances pink and nucleic acids and proteins purple (Debeaujon et al., 2003). For histochemical detection of GUS activity, tissues were incubated in a solution containing 1 mM 5-bromo-4-chloro-3-indolyl-β-D-glucuronide (Phytotechnology Laboratories), 10 mM each of potassium ferrocyanide and potassium ferricyanide, and 10 mM Na_2-EDTA. Vacuum was applied for 10 min before incubating for 16 h at 37°C in the dark. Chlorophyll was removed in 70% (v/v) ethanol:water. To visualize PAs, seeds were stained with 0.5% DMACA solution (0.5% DMACA in absolute ethanol containing 0.8% w/v HCl) for 3 h. Dry seeds were soaked in water for 2 h before staining. Stained seeds were then washed in 70% ethanol for 16 h. For the cross-sectioning, stained tissues were embedded in Paraplast or Technovit 7100 resin after fixation as described above. Observations were performed with a Nikon H550S equipped with bright-field optics.

Promoter Transactivation Assays

Cloning of transcription factor and promoter-reporter constructs in the vector p2GW7 was performed as described (Zhao et al., 2010). For the Gal4 DNA AD (activation domain) fusion, MYB2_m1m2 was cloned into the *Xba*I and *Sma*I restriction sites in frame with the AD in the pMN7 plasmid (Huq et al., 2003). Arabidopsis protoplasts were isolated and transformed as described by Sheen et al. (1995; http://molbio.mgh.harvard.edu/sheenweb/protocols_reg.html). Two micrograms of each plasmid for reporters and

effectors, and 100 ng Renilla luciferase expressing vector (internal control for transfection efficiency) were used to transform 100 μL batches of protoplasts (~1×10^6 cells/mL). The Dual-Luciferase Reporter Assay kit (Promega) was used to quantify the luciferase activities according to the manufacturer's instructions. A GloMax 96 Microplate Luminometer (Promega) was used to read the luciferase activities. For the data analysis, firefly luciferase activities were quantified and normalized to *Renilla* luciferase activities.

BiFC Assays

The constructs for BiFC assays were generated by cloning the indicated genes into Gateway destination vectors pSAT4-DEST-nEYFP-C1 and pSAT5-DEST-cEYFP-C1 (https://www.bio.purdue.edu/people/faculty/gelvin/nsf/protocols_vectors.htm). Arabidopsis

protoplasts were isolated and transfected as described above. Two micrograms of each YFP fusion construct plasmid were used. YFP fluorescence was visualized using a Zeiss LSM10 confocal laser scanning microscope (Zeiss United States), and images were processed with the confocal microscope Zeiss ZEN software.

Statistical Analysis

Statistical analysis was done by Student's *t* test and one-way ANOVA (Microsoft Office Excel 2013). LSD values were calculated using P = 0.05 and used to compare treatment means.

Phylogenetic Analysis

Multiple protein sequence alignments were performed using the ClustalW alignment. The phylogenetic tree was constructed using MEGA 6 (Tamura et al., 2013). Node support was estimated using neighbor-joining bootstrap analysis (1000 bootstrap replicates).

Accession Numbers

Sequence data from this article can be found in the GenBank/EMBL libraries under the following accession numbers: MYB2 (XM_003616340, Medtr5g079670), MYB5 (XM_003601561, Medtr3g083540.1), MYB14 (JN157821, Medtr4g125520.1), WD40-1 (EU040206.1, Medtr3g092840.1), and TT8 (XM_003590608, Medtr1g072320.1).

Supplemental Data

Supplemental Figure 1. Scheme of the flavonoid pathway leading to anthocyanin and PA production in *M. truncatula*.

Supplemental Figure 2. Microarray analysis of *MYB2* (probe set ID Mtr.34401.1.S1_s_at) expression in Mt *LAP1* overexpressing plants of *Medicago sativa*.

Supplemental Figure 3. Protein sequence alignment of R2R3 and R3 domains.

Supplemental Figure 4. Phylogenetic tree of repressor MYB transcription factors based on the entire protein sequences.

Supplemental Figure 5. Protein sequence alignment of Fa MYB1-like proteins and MYBL2.

Supplemental Figure 6. Categorization of probe sets downregulated by MYB2.

Supplemental Figure 7. qRT-PCR analysis of transcript levels in transgenic *MYB2*-overexpressing hairy roots compared with control.

Supplemental Figure 8. Soluble PA levels in wild-type and *myb2* mutant flower and pod.

Supplemental Figure 9. Normal-phase HPLC analysis, with post-column derivatization with DMACA, of soluble PA fractions.

Supplemental Figure 10. Phloroglucinolysis analysis of wild-type (blue) and *myb2-1* (NF10162, red) mutant seeds.

Supplemental Figure 11. Suppression of PA and anthocyanin biosynthesis by *MYB2* overexpression in *Arabidopsis thaliana*.

Supplemental Figure 12. MYB2 interaction with MBW components.

Supplemental Figure 13. TT8-dependent suppression of MYB5 MBW complex activity by MYB2.

Supplemental Figure 14. Dosage-dependent suppression of MBW complex activities by MYB2.

Supplemental Figure 15. Sagittal section of wild-type, *myb2-1* (NF10162), and *wd40-1* seeds at 10 DAP.

Supplemental Figure 16. TBO staining of *wd40-1* mutant seeds.

Supplemental Figure 17. Transverse section of wild-type, *myb2-1* (NF10162), and *wd40-1* seeds across the cotyledon at 10 DAP.

Supplemental Figure 18. Transverse section of wild-type, *myb2-1* (NF10162), and *wd40-1* seeds across the hilum area at 10 DAP.

Supplemental Figure 19. Expression patterns of the $MYB2_{pro}$:*GUS* construct in *M. truncatula*.

Supplemental Table 1. List of oligonucleotide sequences used in this study.

Supplemental Data Set 1. Differentially expressed genes in *MYB2* overexpressing hairy roots.

Supplemental File 1. Text file of alignment corresponding to the phylogenetic analysis in Figure 1B.

Supplemental File 2. Text file of alignment corresponding to the phylogenetic analysis in Supplemental Figure 4.

ACKNOWLEDGMENTS

We thank Jiangqi Wen for screening for *M. truncatula Tnt1* insertion mutants, Yuhong Tang for assistance with microarray analysis, and Stephen Temple for critical reading of the article. This work was supported by Forage Genetics International.

AUTHOR CONTRIBUTIONS

J.H.J., C.L., and R.A.D. designed the research. J.H.J., C.L., and X.X. performed research and analyzed data. J.H.J. and R.A.D. wrote the article.

Received May 29, 2015; revised August 31, 2015; accepted September 10, 2015; published September 28, 2015.

REFERENCES

Abeynayake, S.W., Panter, S., Mouradov, A., and Spangenberg, G. (2011). A high-resolution method for the localization of proanthocyanidins in plant tissues. Plant Methods **7:** 13.

Abrahams, S., Lee, E., Walker, A.R., Tanner, G.J., Larkin, P.J., and Ashton, A.R. (2003). The Arabidopsis TDS4 gene encodes leucoanthocyanidin dioxygenase (LDOX) and is essential for proanthocyanidin synthesis and vacuole development. Plant J. **35:** 624–636.

Aharoni, A., De Vos, C.H., Wein, M., Sun, Z., Greco, R., Kroon, A., Mol, J.N., and O'Connell, A.P. (2001). The strawberry FaMYB1

transcription factor suppresses anthocyanin and flavonol accumulation in transgenic tobacco. Plant J. **28:** 319–332.

Albert, N.W., Davies, K.M., Lewis, D.H., Zhang, H., Montefiori, M., Brendolise, C., Boase, M.R., Ngo, H., Jameson, P.E., and Schwinn, K.E. (2014). A conserved network of transcriptional activators and repressors regulates anthocyanin pigmentation in eudicots. Plant Cell **26:** 962–980.

Albert, N.W., Lewis, D.H., Zhang, H., Irving, L.J., Jameson, P.E., and Davies, K.M. (2009). Light-induced vegetative anthocyanin pigmentation in petunia. J. Exp. Bot. **60:** 2191–2202.

Bassett, M.J., and Miklas, P.N. (2007). A new gene, bic, with pleiotropic effects (with T P V) for bicolor flowers and dark olive brown seed coat in common bean. J. Am. Soc. Hortic. Sci. **132:** 352–356.

Baxter, I.R., Young, J.C., Armstrong, G., Foster, N., Bogenschutz, N., Cordova, T., Peer, W.A., Hazen, S.P., Murphy, A.S., and Harper, J.F. (2005). A plasma membrane H^+-ATPase is required for the formation of proanthocyanidins in the seed coat endothelium of *Arabidopsis thaliana.* Proc. Natl. Acad. Sci. USA **102:** 2649–2654.

Cavallini, E., Matus, J.T., Finezzo, L., Zenoni, S., Loyola, R., Guzzo, F., Schlechter, R., Ageorges, A., Arce-Johnson, P., and Tornielli, G.B. (2015). The phenylpropanoid pathway is controlled at different branches by a set of R2R3-MYB C2 repressors in grapevine. Plant Physiol. **167:** 1448–1470.

Debeaujon, I., Nesi, N., Perez, P., Devic, M., Grandjean, O., Caboche, M., and Lepiniec, L. (2003). Proanthocyanidin-accumulating cells in Arabidopsis testa: regulation of differentiation and role in seed development. Plant Cell **15:** 2514–2531.

Dixon, R.A., Xie, D.Y., and Sharma, S.B. (2005). Proanthocyanidins–a final frontier in flavonoid research? New Phytol. **165:** 9–28.

Dozmorov, I., and Centola, M. (2003). An associative analysis of gene expression array data. Bioinformatics **19:** 204–211.

Dubos, C., Le Gourrierec, J., Baudry, A., Huep, G., Lanet, E., Debeaujon, I., Routaboul, J.M., Alboresi, A., Weisshaar, B., and Lepiniec, L. (2008). MYBL2 is a new regulator of flavonoid biosynthesis in *Arabidopsis thaliana.* Plant J. **55:** 940–953.

Goffard, N., and Weiller, G. (2007). GeneBins: a database for classifying gene expression data, with application to plant genome arrays. BMC Bioinformatics **8:** 87.

Gonzalez, A., Mendenhall, J., Huo, Y., and Lloyd, A. (2009). TTG1 complex MYBs, MYB5 and TT2, control outer seed coat differentiation. Dev. Biol. **325:** 412–421.

Gonzalez, A., Zhao, M., Leavitt, J.M., and Lloyd, A.M. (2008). Regulation of the anthocyanin biosynthetic pathway by the TTG1/bHLH/Myb transcriptional complex in Arabidopsis seedlings. Plant J. **53:** 814–827.

Goodman, C.D., Casati, P., and Walbot, V. (2004). A multidrug resistance-associated protein involved in anthocyanin transport in *Zea mays*. Plant Cell **16:** 1812–1826.

Guimil, S., and Dunand, C. (2006). Patterning of Arabidopsis epidermal cells: epigenetic factors regulate the complex epidermal cell fate pathway. Trends Plant Sci. **11:** 601–609.

Hancock, K.R.D., Collette, V., Fraser, K., Greig, M., Xue, H., Richardson, K., Jones, C., and Rasmussen, S. (2012). Expression of the R2R3-MYB transcription factor TaMYB14 from *Trifolium arvense* activates proanthocyanidin biosynthesis in the legumes *Trifolium repens* and *Medicago sativa.* Plant Physiol. **159:** 1204–1220.

Heppel, S.C., Jaffé, F.W., Takos, A.M., Schellmann, S., Rausch, T., Walker, A.R., and Bogs, J. (2013). Identification of key amino acids for the evolution of promoter target specificity of anthocyanin and proanthocyanidin regulating MYB factors. Plant Mol. Biol. **82:** 457–471.

Hill, K., Wang, H., and Perry, S.E. (2008). A transcriptional repression motif in the MADS factor AGL15 is involved in recruitment of histone deacetylase complex components. Plant J. **53:** 172–185.

Huang, Y.F., Vialet, S., Guiraud, J.L., Torregrosa, L., Bertrand, Y., Cheynier, V., This, P., and Terrier, N. (2014). A negative MYB regulator of proanthocyanidin accumulation, identified through expression quantitative locus mapping in the grape berry. New Phytol. **201:** 795–809.

Huq, E., Al-Sady, B., and Quail, P.H. (2003). Nuclear translocation of the photoreceptor phytochrome B is necessary for its biological function in seedling photomorphogenesis. Plant J. **35:** 660–664.

Irizarry, R.A., Bolstad, B.M., Collin, F., Cope, L.M., Hobbs, B., and Speed, T.P. (2003). Summaries of Affymetrix GeneChip probe level data. Nucleic Acids Res. **31:** e15.

Kagale, S., Links, M.G., and Rozwadowski, K. (2010). Genome-wide analysis of ethylene-responsive element binding factor-associated amphiphilic repression motif-containing transcriptional regulators in Arabidopsis. Plant Physiol. **152:** 1109–1134.

Kazan, K. (2006). Negative regulation of defence and stress genes by EAR-motif-containing repressors. Trends Plant Sci. **11:** 109–112.

Kitamura, S., Matsuda, F., Tohge, T., Yonekura-Sakakibara, K., Yamazaki, M., Saito, K., and Narumi, I. (2010). Metabolic profiling and cytological analysis of proanthocyanidins in immature seeds of *Arabidopsis thaliana* flavonoid accumulation mutants. Plant J. **62:** 549–559.

Koes, R., Verweij, W., and Quattrocchio, F. (2005). Flavonoids: a colorful model for the regulation and evolution of biochemical pathways. Trends Plant Sci. **10:** 236–242.

Kong, Q., Pattanaik, S., Feller, A., Werkman, J.R., Chai, C., Wang, Y., Grotewold, E., and Yuan, L. (2012). Regulatory switch enforced by basic helix-loop-helix and ACT-domain mediated dimerizations of the maize transcription factor R. Proc. Natl. Acad. Sci. USA **109:** E2091–E2097.

Leek, J.T., Monsen, E., Dabney, A.R., and Storey, J.D. (2006). EDGE: extraction and analysis of differential gene expression. Bioinformatics **22:** 507–508.

Lepiniec, L., Debeaujon, I., Routaboul, J.M., Baudry, A., Pourcel, L., Nesi, N., and Caboche, M. (2006). Genetics and biochemistry of seed flavonoids. Annu. Rev. Plant Biol. **57:** 405–430.

Li, C., and Wong, W.H. (2001). Model-based analysis of oligonucleotide arrays: expression index computation and outlier detection. Proc. Natl. Acad. Sci. USA **98:** 31–36.

Li, S.F., Milliken, O.N., Pham, H., Seyit, R., Napoli, R., Preston, J., Koltunow, A.M., and Parish, R.W. (2009). The Arabidopsis MYB5 transcription factor regulates mucilage synthesis, seed coat development, and trichome morphogenesis. Plant Cell **21:** 72–89.

Liu, C., Jun, J.H., and Dixon, R.A. (2014). MYB5 and MYB14 play pivotal roles in seed coat polymer biosynthesis in *Medicago truncatula.* Plant Physiol. **165:** 1424–1439.

Matsui, K., Umemura, Y., and Ohme-Takagi, M. (2008). AtMYBL2, a protein with a single MYB domain, acts as a negative regulator of anthocyanin biosynthesis in Arabidopsis. Plant J. **55:** 954–967.

Mouradov, A., and Spangenberg, G. (2014). Flavonoids: a metabolic network mediating plants adaptation to their real estate. Front. Plant Sci. **5:** 620.

Nemie-Feyissa, D., Olafsdottir, S.M., Heidari, B., and Lillo, C. (2014). Nitrogen depletion and small R3-MYB transcription factors affecting anthocyanin accumulation in Arabidopsis leaves. Phytochemistry **98:** 34–40.

Pang, Y., Peel, G.J., Wright, E., Wang, Z., and Dixon, R.A. (2007). Early steps in proanthocyanidin biosynthesis in the model legume *Medicago truncatula.* Plant Physiol. **145:** 601–615.

Pang, Y., Peel, G.J., Sharma, S.B., Tang, Y., and Dixon, R.A. (2008). A transcript profiling approach reveals an epicatechin-specific glucosyltransferase expressed in the seed coat of *Medicago truncatula.* Proc. Natl. Acad. Sci. USA **105:** 14210–14215.

Pang, Y., et al. (2009). A WD40 repeat protein from *Medicago truncatula* is necessary for tissue-specific anthocyanin and proanthocyanidin biosynthesis but not for trichome development. Plant Physiol. **151:** 1114–1129.

Paolocci, F., Robbins, M.P., Passeri, V., Hauck, B., Morris, P., Rubini, A., Arcioni, S., and Damiani, F. (2011). The strawberry transcription factor FaMYB1 inhibits the biosynthesis of proanthocyanidins in *Lotus corniculatus* leaves. J. Exp. Bot. **62:** 1189–1200.

Peel, G.J., and Dixon, R.A. (2007). Detection and quantification of engineered proanthocyanidins in transgenic plants. Nat. Prod. Commun. **2:** 1009–1014.

Peel, G.J., Pang, Y., Modolo, L.V., and Dixon, R.A. (2009). The LAP1 MYB transcription factor orchestrates anthocyanidin biosynthesis and glycosylation in Medicago. Plant J. **59:** 136–149.

Poustka, F., Irani, N.G., Feller, A., Lu, Y., Pourcel, L., Frame, K., and Grotewold, E. (2007). A trafficking pathway for anthocyanins overlaps with the endoplasmic reticulum-to-vacuole protein-sorting route in Arabidopsis and contributes to the formation of vacuolar inclusions. Plant Physiol. **145:** 1323–1335.

Ramsay, N.A., and Glover, B.J. (2005). MYB-bHLH-WD40 protein complex and the evolution of cellular diversity. Trends Plant Sci. **10:** 63–70.

Reed, J.D. (1995). Nutritional toxicology of tannins and related polyphenols in forage legumes. J. Anim. Sci. **73:** 1516–1528.

Salvatierra, A., Pimentel, P., Moya-León, M.A., and Herrera, R. (2013). Increased accumulation of anthocyanins in *Fragaria chiloensis* fruits by transient suppression of FcMYB1 gene. Phytochemistry **90:** 25–36.

Schiefelbein, J. (2003). Cell-fate specification in the epidermis: a common patterning mechanism in the root and shoot. Curr. Opin. Plant Biol. **6:** 74–78.

Sharma, S.B., and Dixon, R.A. (2005). Metabolic engineering of proanthocyanidins by ectopic expression of transcription factors in *Arabidopsis thaliana*. Plant J. **44:** 62–75.

Sheen, J., Hwang, S., Niwa, Y., Kobayashi, H., and Galbraith, D.W. (1995). Green-fluorescent protein as a new vital marker in plant cells. Plant J. **8:** 777–784.

Shen, H., He, X., Poovaiah, C.R., Wuddineh, W.A., Ma, J., Mann, D.G., Wang, H., Jackson, L., Tang, Y., Stewart, C.N., Jr., Chen, F., and Dixon, R.A. (2012). Functional characterization of the switchgrass (*Panicum virgatum*) R2R3-MYB transcription factor PvMYB4 for improvement of lignocellulosic feedstocks. New Phytol. **193:** 121–136.

Smýkal, P., Vernoud, V., Blair, M.W., Soukup, A., and Thompson, R.D. (2014). The role of the testa during development and in establishment of dormancy of the legume seed. Front. Plant Sci. **5:** 351.

Steyn, W.J., Wand, S.J.E., Holcroft, D.M., and Jacobs, G. (2002). Anthocyanins in vegetative tissues: a proposed unified function in photoprotection. New Phytol. **155:** 349–361.

Tadege, M., Wen, J., He, J., Tu, H., Kwak, Y., Eschstruth, A., Cayrel, A., Endre, G., Zhao, P.X., Chabaud, M., Ratet, P., and Mysore, K.S. (2008). Large-scale insertional mutagenesis using the Tnt1 retrotransposon in the model legume *Medicago truncatula*. Plant J. **54:** 335–347.

Tamura, K., Stecher, G., Peterson, D., Filipski, A., and Kumar, S. (2013). MEGA6: Molecular Evolutionary Genetics Analysis version 6.0. Mol. Biol. Evol. **30:** 2725–2729.

Tanner, G.J., Francki, K.T., Abrahams, S., Watson, J.M., Larkin, P.J., and Ashton, A.R. (2003). Proanthocyanidin biosynthesis in plants. Purification of legume leucoanthocyanidin reductase and molecular cloning of its cDNA. J. Biol. Chem. **278:** 31647–31656.

Tuteja, J.H., Clough, S.J., Chan, W.C., and Vodkin, L.O. (2004). Tissue-specific gene silencing mediated by a naturally occurring chalcone synthase gene cluster in *Glycine max.* Plant Cell **16:** 819–835.

Verdier, J., Zhao, J., Torres-Jerez, I., Ge, S., Liu, C., He, X., Mysore, K.S., Dixon, R.A., and Udvardi, M.K. (2012). MtPAR MYB transcription factor acts as an on switch for proanthocyanidin biosynthesis in *Medicago truncatula*. Proc. Natl. Acad. Sci. USA **109:** 1766–1771.

Voß, U., Bishopp, A., Farcot, E., and Bennett, M.J. (2014). Modelling hormonal response and development. Trends Plant Sci. **19:** 311–319.

Xie, D.Y., Sharma, S.B., Paiva, N.L., Ferreira, D., and Dixon, R.A. (2003). Role of anthocyanidin reductase, encoded by BANYULS in plant flavonoid biosynthesis. Science **299:** 396–399.

Xu, W., Lepiniec, L., and Dubos, C. (2014). New insights toward the transcriptional engineering of proanthocyanidin biosynthesis. Plant Signal. Behav. **9:** e28736.

Ye, H., Li, L., Guo, H., and Yin, Y. (2012). MYBL2 is a substrate of GSK3-like kinase BIN2 and acts as a corepressor of BES1 in brassinosteroid signaling pathway in Arabidopsis. Proc. Natl. Acad. Sci. USA **109:** 20142–20147.

Yoshida, K., Ma, D., and Constabel, C.P. (2015). The MYB182 protein down-regulates proanthocyanidin and anthocyanin biosynthesis in poplar by repressing both structural and regulatory flavonoid genes. Plant Physiol. **167:** 693–710.

Zhang, H., Wang, L., Deroles, S., Bennett, R., and Davies, K. (2006). New insight into the structures and formation of anthocyanic vacuolar inclusions in flower petals. BMC Plant Biol. **6:** 29.

Zhao, J., and Dixon, R.A. (2009). MATE transporters facilitate vacuolar uptake of epicatechin 3′-*O*-glucoside for proanthocyanidin biosynthesis in *Medicago truncatula* and Arabidopsis. Plant Cell **21:** 2323–2340.

Zhao, Q., Wang, H., Yin, Y., Xu, Y., Chen, F., and Dixon, R.A. (2010). Syringyl lignin biosynthesis is directly regulated by a secondary cell wall master switch. Proc. Natl. Acad. Sci. USA **107:** 14496–14501.

Zhu, H.F., Fitzsimmons, K., Khandelwal, A., and Kranz, R.G. (2009). CPC, a single-repeat R3 MYB, is a negative regulator of anthocyanin biosynthesis in Arabidopsis. Mol. Plant **2:** 790–802.

Zimmermann, I.M., Heim, M.A., Weisshaar, B., and Uhrig, J.F. (2004). Comprehensive identification of *Arabidopsis thaliana* MYB transcription factors interacting with R/B-like BHLH proteins. Plant J. **40:** 22–34.